ORIGINAL RESEARCH

Integrins $\alpha_v\beta_5$ and $\alpha_v\beta_6$ Mediate IL-4–induced Collective Migration in Human Airway Epithelial Cells

Sang-Nam Lee[1], Ji-Suk Ahn[1], Seong Gyu Lee[2], Hyung-Suk Lee[2], Augustine M. K. Choi[3,4], and Joo-Heon Yoon[1,5]

[1]The Airway Mucus Institute and [5]Department of Otorhinolaryngology, Yonsei University College of Medicine, Seoul, Korea; [2]School of Mechanical Engineering, Yonsei University, Seoul, Korea; [3]Joan and Sanford I. Weill Department of Medicine, Weill Cornell Medical College and New York-Presbyterian Hospital, New York, New York; and [4]Division of Pulmonary and Critical Care Medicine, Weill Cornell Medical College, New York, New York

Abstract

A positive link between persistent cellular motion and a defective tight junction barrier allows increased antigenic penetration and contact between ligand–receptor pairs, leading to exacerbated allergic airway inflammation and remodeling. Given that collective cell migration involves cell–cell and cell–extracellular matrix adhesions, and given that IL-4 induces epithelial barrier dysfunction and decreases cell–extracellular matrix adhesions, we hypothesized that IL-4 may induce collective migration in the well-differentiated primary human nasal epithelial cells (HNECs). Well-differentiated HNECs were treated with IL-4, and the effects of IL-4 on cell migration were investigated using genetic and pharmacological approaches, live-cell imaging, a vertex model, and immunostaining. IL-4 disrupted the expression and localization of the tight junction proteins zonula occludens 1 and occludin, and it induced the cleavage and asymmetric distribution of E-cadherin in the HNEC layers. It also induced collective epithelial migration and cell shape changes driven by actin cytoskeleton reorganization. In addition, the effect of IL-4 on collective HNEC migration was reversed by pharmacologic and genetic inhibition of the α_v-integrin–activating enzyme furin, and function-blocking antibodies for $\alpha_v\beta_5$ or $\alpha_v\beta_6$. In IL-4–stimulated cells, both anti-$\alpha_v\beta_5$ and anti-$\alpha_v\beta_6$ inhibited the phosphorylation of focal adhesion kinase. Furthermore, both β_5- and β_6-integrins were enriched in basal cells in the injured airway epithelium with allergic rhinitis. These findings suggest that $\alpha_v\beta_5$ and $\alpha_v\beta_6$ serve as critical mechanoreceptors in IL-4–induced collective HNEC migration through the focal adhesion kinase signaling pathway. These results have implications for targeting treatment of exacerbation of respiratory allergic diseases.

Keywords: collective cell migration; cultured human nasal epithelial cells; furin; integrin; IL-4

Epithelial damage and remodeling are characteristic features of allergic airway diseases such as allergic rhinitis (AR) and asthma (1, 2). Pseudostratified airway epithelium containing basal (BL), mucous, and ciliated cells is frequently injured through exposure to inhaled noxious and pathogenic agents or inflammatory mediators (3). Therefore, epithelial wound repair characterized by basal cell (BC) spreading and migration, followed by proliferation and differentiation, is an important process during which epithelial barrier integrity is rapidly restored (3). In the mature polarized epithelium, tight junction (TJ) complexes are critical for the formation of epithelial apicobasal polarity by controlling the distribution of proteins to apical (AP) or basolateral membrane domains and establishing a paracellular diffusion barrier between the two by

(Received in original form March 7, 2018; accepted in final form October 18, 2018)

Supported by Global Research Laboratory (GRL) Program of the National Research Foundation of Korea (NRF), funded by the Ministry of Science, Information and Communication Technologies (ICT) and Future Planning (2016K1A1A2910779 [J.-H.Y. and A.M.K.C.]), and by the Basic Science Research Program through the NRF, funded by the Ministry of Education (2016R1D1A1B01007747 [S.-N.L.]).

Author Contributions: S.-N.L. and J.-H.Y.: designed the studies and experiments; S.-N.L., J.-S.A., and S.G.L.: performed the experiments; S.-N.L., H.-S.L., A.M.K.C., and J.-H.Y.: contributed new analytic tools; S.-N.L., J.-S.A., S.G.L., H.-S.L., A.M.K.C., and J.-H.Y.: interpreted the data; and S.N.L. and J.H.Y.: wrote the manuscript. All the authors read and approved the final manuscript.

Correspondence and requests for reprints should be addressed to Joo-Heon Yoon, M.D., Department of Otorhinolaryngology, Yonsei University College of Medicine, 50-1 Yonsei-ro, Seodaemun-gu, Seoul 03722, Korea. E-mail: jhyoon@yuhs.ac.

This article has a data supplement, which is accessible from this issue's table of contents at www.atsjournals.org.

Am J Respir Cell Mol Biol Vol 60, Iss 4, pp 420–433, Apr 2019
Copyright © 2019 by the American Thoracic Society
Originally Published in Press as DOI: 10.1165/rcmb.2018-0081OC on October 25, 2018
Internet address: www.atsjournals.org

limiting solute passage (4, 5). However, persistent TJ barrier disruption could allow penetration of inhaled allergens or particles and contact of ligand–receptor pairs normally segregated in either the AP or basolateral membrane domain, resulting in sustained activation of signaling pathways that affect the expression of specific genes and the production of extracellular matrix (ECM) molecules (4, 5). Finally, the airway epithelial barrier dysfunction may lead to aberrant airway remodeling including epithelial cell shedding, BC and mucous cell hyperplasia, and increased and abnormal ECM protein deposition (2, 3).

During early-phase tissue remodeling events in embryonic development, wound repair, and cancer, cells move as a large cell cluster by maintaining strong E-cadherin–mediated cell–cell adhesion, referred to as "collective migration" (6, 7). The leader cells in a migrating cluster exhibit highly motile mesenchymal properties, including actin cytoskeleton reorganization, defective TJ function, and altered cellular polarity (6, 7). Because epithelial cells are mechanically coupled to the actin cytoskeleton at E-cadherin–based adherens junctions (AJs) and integrin-mediated focal contacts, a coordinated cross-talk between E-cadherin and integrins transmits physical force and biomechanical signals to neighboring cells and the ECM, and a fine balance of tension across these two adhesion systems is pivotal for directional collective cell migration (8). Integrins are the major transmembrane receptors for ECM proteins that regulate cell migration though focal adhesion kinase (FAK) signaling (9). They are composed of noncovalently linked α- and β-subunits; in humans, at least 18 α- and 8 β-subunits have been identified, forming 24 heterodimers with different cell expression patterns and ligand specificities. Human airway epithelial cells express eight different integrins: $\alpha_2\beta_1$, $\alpha_3\beta_1$, $\alpha_5\beta_1$, $\alpha_6\beta_4$, $\alpha_9\beta_1$, $\alpha_v\beta_5$, $\alpha_v\beta_6$, and $\alpha_v\beta_8$ (10). Pilewski and colleagues reported that in an *in vivo* model of human airway epithelial wound repair, epithelial cells exhibited sustained upregulation of $\alpha_v\beta_5$ and $\alpha_v\beta_6$, transient upregulation of $\alpha_5\beta_1$, and altered distribution of $\alpha_2\beta_1$ and $\alpha_6\beta_4$ (11). They also showed that expression of α_v-, β_5-, and α_5-integrins, but not β_6-integrin, is detected on basal epithelial cells in normal epithelium, whereas expression of α_v-, β_5-, and β_6-integrins, but not α_5-integrin, is increased in undifferentiated epithelium from patients with cystic fibrosis (11). In addition, α_v-coupled β-integrins (β_1-, β_3-, β_5-, and β_6-integrins) positively control FAK expression and activation (12, 13). Interestingly, α_v-integrin undergoes endoproteolytic cleavage by proprotein convertases (PCs) to become biologically active (14). So far, seven mammalian PCs have been identified: furin, paired basic amino acid–cleaving enzyme 4 (PACE4), PC1/3, PC2, PC4, PC5/6, and PC7 (15). We previously demonstrated the presence of furin and PACE4 in primary human nasal epithelial cells (HNECs) (16, 17).

Previous studies showed that IL-4 and IL-13, essential mediators in T-helper type 2 (Th2)-driven allergic inflammation, disrupt epithelial barrier integrity through decreased expression of the TJ proteins zonula occludens 1 (ZO-1) and occludin, increased epithelial permeability, and reduced adhesions of epithelial cells to the ECM, all of which are required for cell migration initiation (2, 18–20). Indeed, IL-4 appears to accelerate airway epithelial cell migration after mechanical injury, thereby enhancing wound repair (21). However, the effect of IL-4 on collective migration in the primary well-differentiated HNEC layers grown at the air–liquid interface (ALI) (22) with a similar physiological condition of naive airway epithelium (22) has not been elucidated. Interestingly, Park and colleagues recently showed that applying compressive stress mimicking asthmatic bronchospasm to primary human bronchial epithelial cells in ALI culture induced collective cellular motions that exhibited a transition from a nonmotile, jammed, solid-like state to a motile, unjammed, fluid-like state (23).

In the present study, we investigated the role of integrins $\alpha_v\beta_5$ and $\alpha_v\beta_6$ in IL-4–induced collective migration in the well-differentiated HNEC layers. Our experiments using genetic and pharmacological approaches with sophisticated live-cell imaging provide evidence that IL-4 induces collective migration in the HNEC layers, that furin inhibition suppresses pro–α_v-integrin processing, and that integrins $\alpha_v\beta_5$ and $\alpha_v\beta_6$ mediate IL-4–induced collective migration in the HNEC layers via an FAK signaling pathway.

Methods

Details of the methods are fully described in the data supplement.

Ethics Statement

The institutional review board of Yonsei University College of Medicine approved the study protocols (IRB 4-2016-1153). Nasal mucosa were harvested from a portion of the inferior turbinate during turbinoplasty. AR was diagnosed on the basis of a history of allergic symptoms, including nasal congestion, itchy sensation, rhinorrhea, or sneezing, and a positive multiple-allergen simultaneous test result (allergen-specific IgE concentration class $\geq$2).

Results

IL-4 Induces Disruption of TJ Proteins and Cleavage and Asymmetric Distribution of E-Cadherin in the Well-Differentiated HNEC Layers

Because disruption of TJ proteins and intercellular remodeling of E-cadherin–based AJs are required for the collective cell migration (6, 7), we first determined whether IL-4 can disrupt the function of TJ proteins and E-cadherin in the well-differentiated HNEC layers. HNECs differentiated at the ALI culture for 2 weeks were treated with different concentrations of IL-4 (0–20 ng/ml) to the basolateral compartment for 24 hours. The protein concentrations and localization of TJ proteins and E-cadherin were determined by Western blotting and immunofluorescent staining, respectively. The expression levels of ZO-1 and occludin in HNECs were dose dependently decreased by IL-4 (Figure 1A), indicating that IL-4 disrupts TJ function; the most effective dose was 5 ng/ml. Immunofluorescence analysis revealed that untreated controls exhibited ZO-1 localization at the intercellular junctions, whereas IL-4–stimulated HNECs displayed redistribution of ZO-1 from the intercellular junctions into the intracellular compartment as well as disruption of TJ integrity, as judged by the discontinuities in ZO-1 ring structures (Figure 1B). Interestingly, full-length E-cadherin was cleaved by IL-4 stimulation in a dose-dependent manner, generating a 38 kD C-terminal fragment (Figure 1C). In

addition, E-cadherin immunoreactivity was very prominent at cell junctions of untreated controls, whereas IL-4 stimulation induced asymmetric localization of E-cadherin at different sides of HNECs, resulting in decreased affinities between adjacent cells (Figure 1D). We also observed the formation of a refined boundary between adjacent cell populations in the IL-4–stimulated HNEC layers (Figure 1D), suggesting that IL-4 induces separation of different cell clusters by the affinity of their E-cadherin–mediated adhesions in the HNEC layers. Taken together, TJ barrier disruption and E-cadherin–based AJ remodeling in the IL-4–stimulated HNEC layers may promote collective migration of HNECs.

IL-4 Induces the Alteration of Cell Shape and Actin Cytoskeleton Organization in HNECs

Changes in cell shape and actin cytoskeleton organization systematically drive cellular rearrangements and motility (23, 24). We therefore determined whether IL-4 can induce the alteration of cell shape and actin cytoskeleton organization in the well-differentiated HNEC layers. Of note, the well-differentiated HNECs form organized, multilayered epithelial structures containing AP differentiated cells and basilar undifferentiated BCs (25). HNECs were treated with IL-4 to the basolateral compartment for 24 hours; actin filaments were visualized with FITC-phalloidin; and cell shape changes were monitored at both AP and BL levels of the HNEC layers (Figure 2). Confocal images of x–z sections of the IL-4–stimulated HNEC layers revealed actin cytoskeleton reorganization of BCs, compared with that of untreated controls (Figure 2A). Consistently, confocal x–y images at the BL-I level of the IL-4–stimulated HNEC layers displayed the morphological alteration of BCs from their typical cobblestone (Figure 2B, upper panel, left) to spindle shape (Figure 2B, lower panel, left), and x–y images at the BL-II level showed actin cytoskeleton reorganization with the formation of an extensive network of actin fibers in BCs (Figure 2B, lower panel, right). These data suggest that IL-4–stimulated BCs undergo epithelial–mesenchymal transition (EMT)-like changes. Indeed, expression of EMT markers ACTA2 and vimentin (26) was significantly increased in IL-4–stimulated HNECs compared with untreated controls (Figure 2C).

We also observed that the AP confocal plane of the untreated controls exhibited a relatively ordered polygonal packing pattern with edges shared between neighboring cells, whereas IL-4–stimulated HNECs showed more irregular and elongated shapes (Figure 2D, left panels). In the vertex model that links cell mechanics to cell shape and cell motility, the AP cell shapes of the confluent layer are determined by the competition between cell–cell adhesion and contractile cortical tension, generating an effective cell shape index p_0 (ratio of the cell perimeter to the square root of the cell area) (22). This parameter serves as a rigorous structural signature in determining whether cells are in a nonmotile, jammed, solid-like state or a motile, unjammed, fluid-like state (23, 24). To assess whether the jammed-to-unjammed transition of the IL-4–stimulated HNEC layers was present, we determined the cell shape index for individual cells in the layers using the vertex model. Cell boundaries were manually traced over the fluorescently labeled actin images of HNECs acquired from the confocal microscope, and cell shapes were analyzed using a custom MATLAB script (MathWorks) (Figure 2D, right panels). Note that the jammed-to-unjammed transition of the cellular collective occurs at a critical value of $p_0 \approx 3.81$ ($p_0{}^*$) (23, 24). The data revealed that the median of p_0 for untreated controls was 3.80, corresponding to a jammed state, whereas the median of p_0 for IL-4–stimulated cells was 4.56, corresponding to an unjammed state (Figure 2E), indicating that IL-4 induced the jammed-to-unjammed transition in the HNEC layers.

Previously, it was demonstrated that FAK is a crucial mediator of integrin signaling that is localized to focal adhesions (9). In response to detachment from the ECM, FAK is rapidly dephosphorylated at Tyr397, which is accompanied by refractile morphological changes and loss of focal adhesions, followed by integrin-mediated phosphorylation of FAK at Tyr397 (pFAK-Y397) and Tyr925 (pFAK-Y925) for the reattachment of the cells to the ECM and the focal adhesion turnover during subsequent cell migration (9). Western blot analysis in the present study showed that IL-4 significantly increased the concentrations of pFAK-Y397 and pFAK-Y925 (Figure 2F). Collectively, these data suggest that IL-4 can induce collective migration in the well-differentiated HNEC layers via integrin-mediated FAK signaling.

IL-4 Induces Initial Transient Contraction of the HNEC Layers from the Leading Front after Injury

IL-4 decreases cell–cell and cell–ECM interactions (2, 18–20); epithelial cells are mechanically coupled to the actin cytoskeleton at E-cadherin–based AJs and integrin-mediated focal contacts (6–8, 27, 28); and release of tension exerted by cells on the ECM after actin cytoskeleton collapse and loss of cell surface triggers transient cell hypercontraction (29, 30). Therefore, we hypothesized that IL-4 may induce the transient contraction of the HNEC layers and so may trigger the initiation of collective cellular motion by pushing and pulling from the surrounding cells in a confluent layer. To test this hypothesis, the well-differentiated HNEC layers were wounded with an approximately 1-mm-wide scratch across the diameter of the well before IL-4 addition in the basolateral compartment. Wound closure was monitored with time-lapse microscopy for 18 hours at 3-minute intervals (*see* Movies E1 and E2 in the data supplement). Upon scratching, both control and IL-4–stimulated cells revealed coordinated, directed progression of the leading front of an epithelial sheet, and similarly to a previous study (21), IL-4 accelerated HNEC migration compared with untreated controls (Figures 3A and 3B). Surprisingly, we observed that IL-4–stimulated cells migrated in the opposite direction during the early phase after wounding (Figure 3B). We then calculated the migration speed of HNECs in the layers as a function of their distance to the edge over the first 6 hours after wounding using particle image velocimetry. As expected, IL-4–stimulated cells displayed significant negative velocities during approximately 1 hour after wounding (Figures 3C and 3D), indicating initial transient contraction of the epithelial sheet from the wound edge, possibly due to reduction of integrin-based cell–ECM adhesions by IL-4 treatment. Interestingly, IL-4 significantly attenuated the concentrations of pFAK-Y397 and pFAK-Y925 by 2 hours post-stimulation

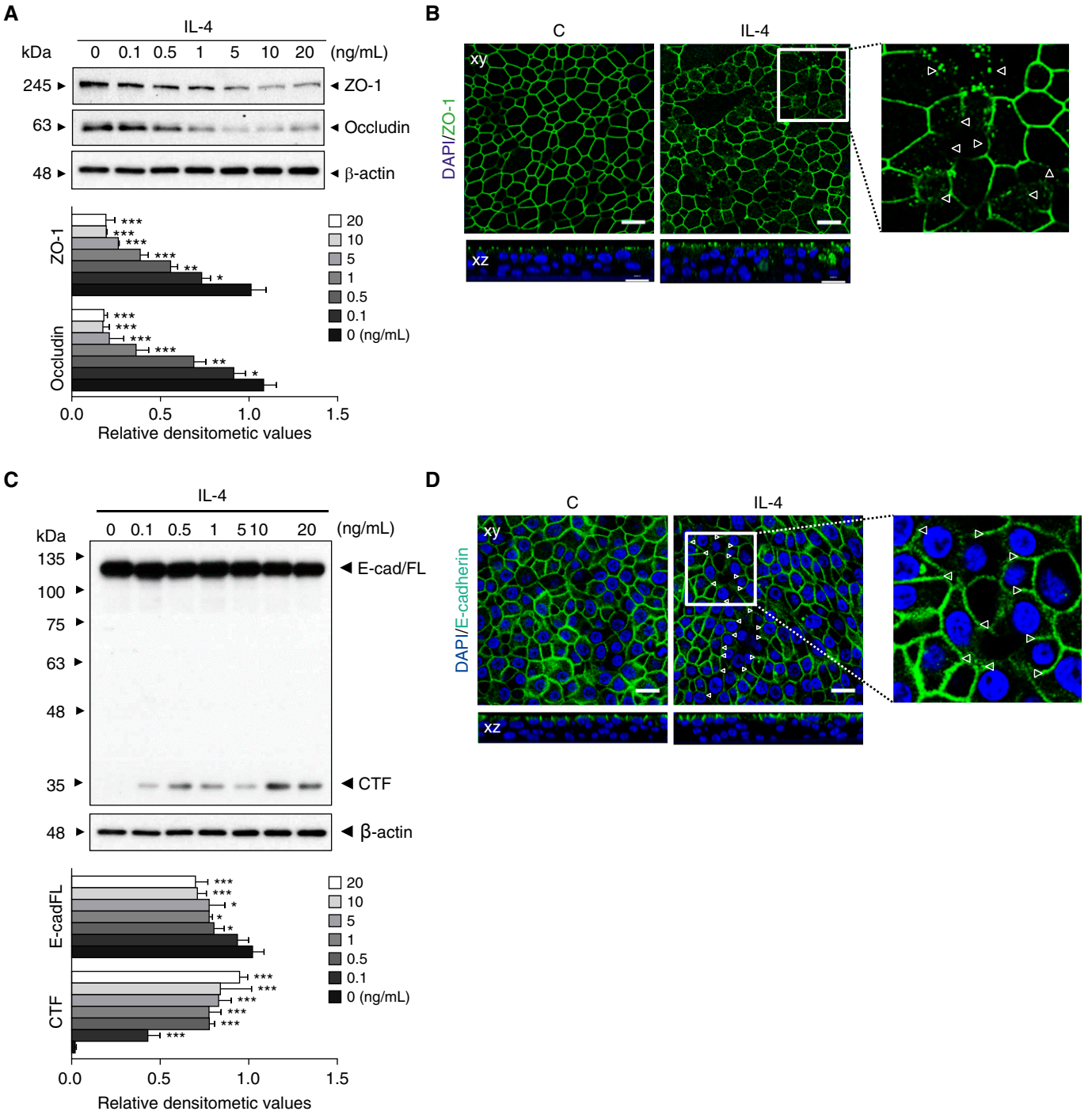


Figure 1. IL-4 alters the expression and localization of tight junction protein and induces the cleavage and asymmetric localization of E-cadherin in the human nasal epithelial cell layers. Human nasal epithelial cells (HNECs) differentiated at the air–liquid interface culture for 2 weeks were treated with different IL-4 concentrations (0–20 ng/ml) in the basolateral compartment for 24 hours. (*A*) Zonula occludens 1 (ZO-1) and occludin expression were examined by Western blotting. Bottom panel shows densitometric data from the blots ($n = 3$). Samples were normalized to β-actin content, and results are presented as mean ± SD. $^{*}P < 0.01$, $^{**}P < 0.001$, and $^{***}P < 0.0001$ versus untreated controls by one-way ANOVA. (*B*) Untreated control and 5 ng/ml IL-4–treated cells were immunostained for ZO-1 (green) and DAPI (nuclei, blue). Confocal *x–y* and *x–z* sections are shown. The white boxed area in the middle panel is shown at a higher magnification in the right panel. The open arrowheads point to regions where ZO-1 staining is discontinuous. Scale bars: 20 μm. (*C*) E-cadherin expression was examined by Western blotting. Relative densitometric values are shown in the bottom panel. Data are presented as mean ± SD ($n = 3$). $^{*}P < 0.01$ and $^{***}P < 0.0001$ versus untreated controls by one-way ANOVA. (*D*) Representative immunofluorescence images of untreated control and IL-4–treated cells stained with E-cadherin (green) and DAPI (blue). The open arrowheads indicate well-established boundaries between clusters. The white boxed area in the middle panel is shown at a higher magnification in the right panel. Scale bars: 20 μm. C = control; CTF = C-terminal fragment of E-cadherin; E-Cad/FL = full-length E-cadherin.

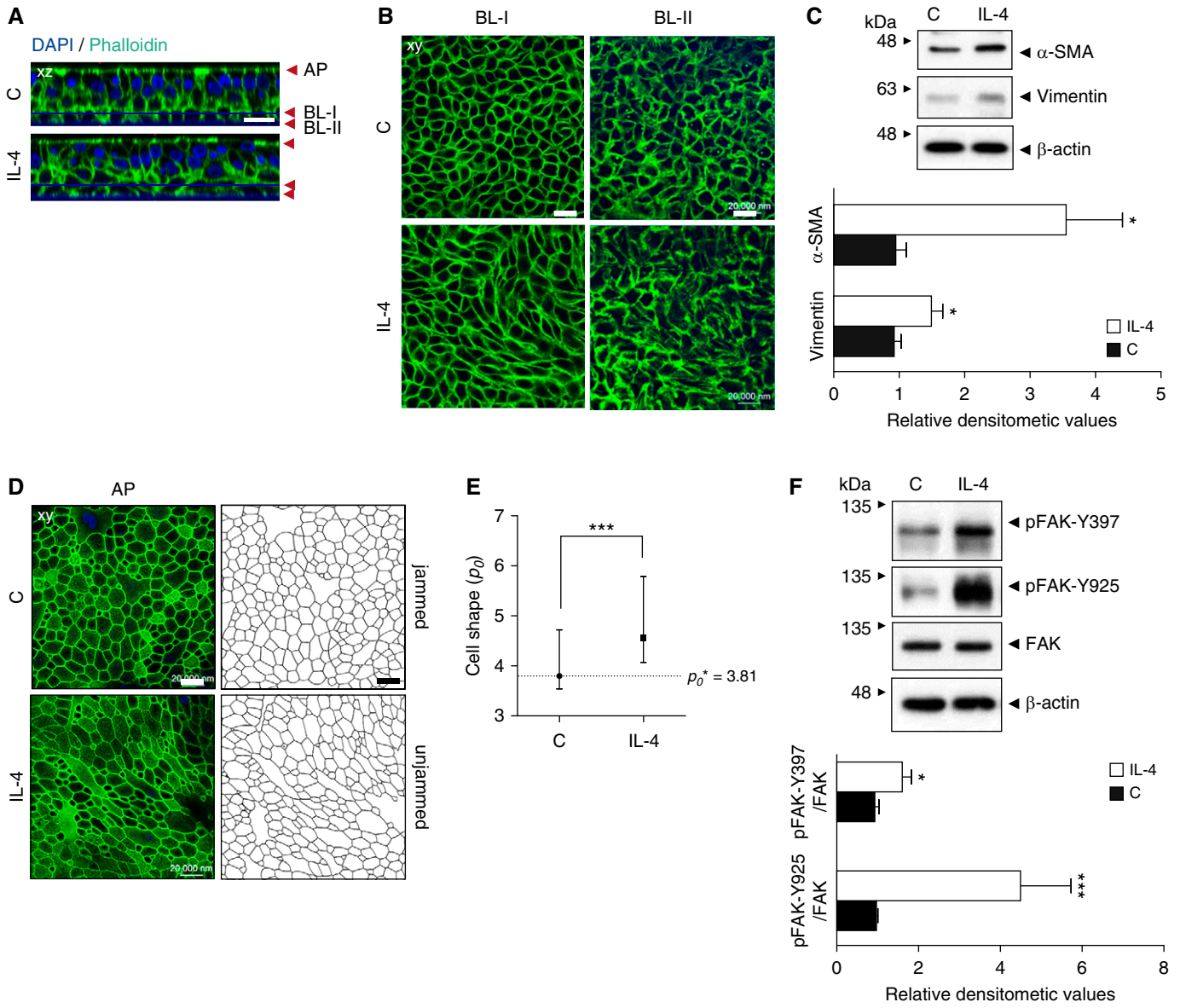


Figure 2. IL-4 alters cell shape and actin cytoskeleton organization in the confluent human nasal epithelial cell layers. Well-differentiated HNECs were treated with IL-4 (5 ng/ml) for 24 hours, and F-actin (green) was visualized by FITC-phalloidin staining. (*A*) Representative immunofluorescence images of confocal *x–z* sections of the HNEC layers. (*B*) Confocal *x–y* sections at the basal level (BL-I and BL-II, indicated by the arrowhead in *A*) of the HNEC layers. Note that *x–y* images at the BL-I level display junctional actin morphology at the apicolateral region of basal cells and *x–y* images at the BL-II level show actin stress fibers on the basal side of cells. Scale bars: 20 μm. (*C*) Cell lysates were immunoblotted with antibodies to epithelial–mesenchymal transition markers ACTA2 (α-SMA) and vimentin. Bottom panel shows densitometric data from the blots ($n = 3$). Samples were normalized to β-actin content, and results are presented as mean ± SD. $^*P < 0.01$ versus untreated controls by one-way ANOVA. (*D*) Confocal *x–y* sections at the apical (AP) level of the HNEC layers (left panels). For quantification of cell shapes using the vertex model, cell boundaries were manually traced over the fluorescently labeled actin images of HNECs acquired from the confocal microscope (right panels). Cell shapes were analyzed using a custom MATLAB script. Scale bars: 20 μm. (*E*) The median of p_0 for untreated controls was 3.85, indicating that the cell layer becomes solid-like and jammed. In contrast, the median of p_0 for IL-4–stimulated cells was 4.63, indicating that the layer becomes fluid-like and unjammed. Plot shows median with range. $^{***}P < 0.0001$ by Student's *t* test. (*F*) The expression of pFAK-Y397, pFAK-Y925, and focal adhesion kinase (FAK) was examined by Western blotting. Bottom panel shows densitometric data from the blots ($n = 3$). Samples were normalized to β-actin content, and results are presented as mean ± SD. $^*P < 0.01$ and $^{***}P < 0.0001$ versus untreated controls by one-way ANOVA. p = phospho.

compared with no treatment (Figure 3E), suggesting that IL-4 induces transient contraction of the HNEC layers in the early phase of wound repair, possibly by reducing FAK phosphorylation. Taken together, these results suggest that transient cellular contractility and mechanical stresses arising from an IL-4–induced imbalance of E-cadherin–mediated cell–cell and integrin-based cell–ECM interactions can trigger and accelerate collective migration of HNECs in a confluent layer.

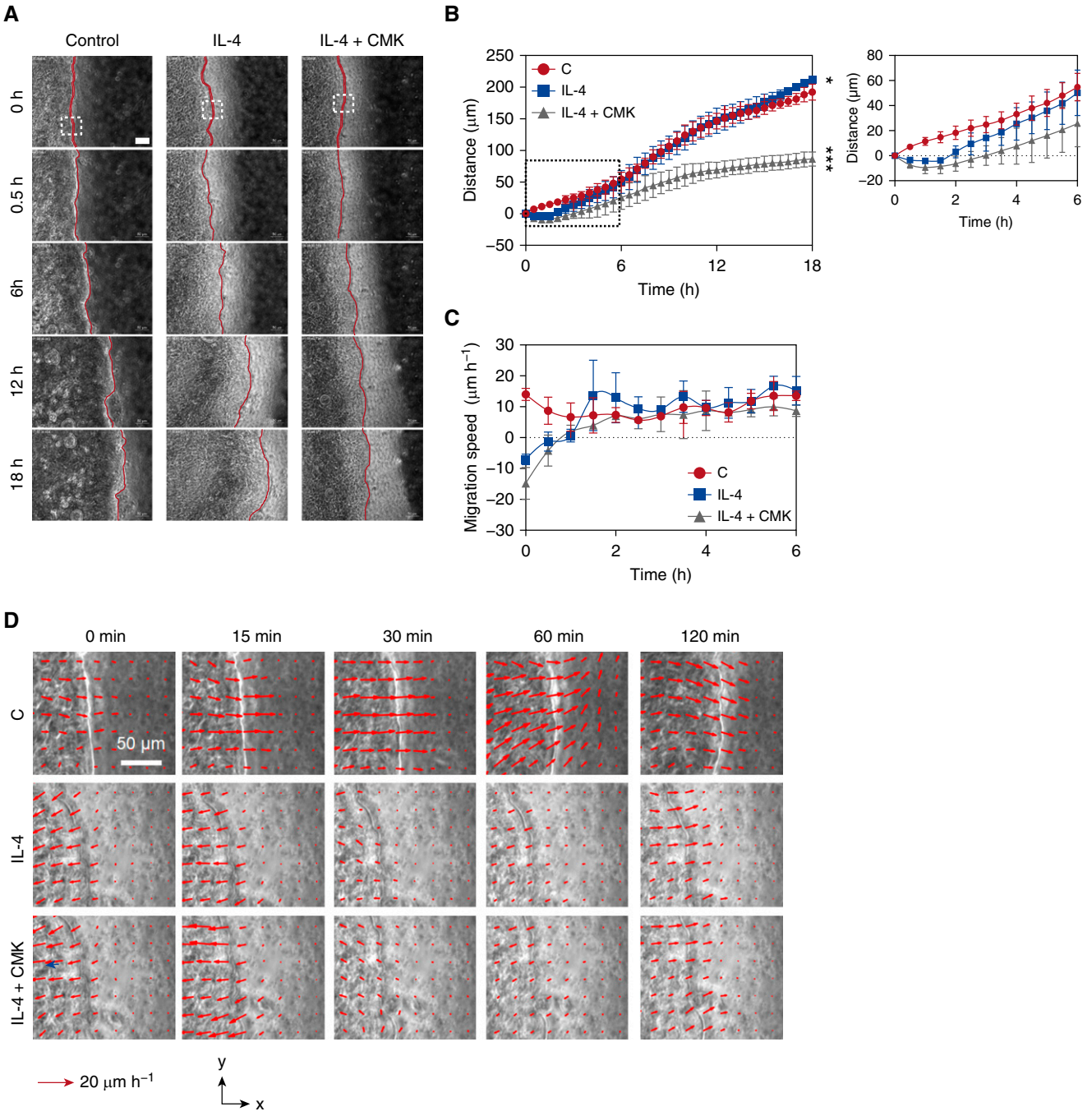


Figure 3. IL-4 induces initial transient contraction of the HNEC layers from the leading front after mechanical injury by suppressing FAK phosphorylation. Well-differentiated HNECs were wounded with a sterile 200-μl pipette tip by one perpendicular linear scratch before the addition of IL-4 (5 ng/ml) with or without decanoyl-RVKR-chloromethylketone (CMK) (25 μM). Immediately after wounding, cells were tracked using time-lapse video microscopy for 18 hours at 3-minute intervals. Time-lapse difference images were calculated for the displacement and velocity of the leading front. (*A*) Representative images taken at the indicated time points after wounding are displayed. Scale bar: 50 μm. (*B*) HNEC layer edge evolution over 18 hours. The position of the migrating cell sheet boundary along the *x*-axis was traced at three different *y*-axis positions. Magnification of the region indicated by the box in the left panel is shown in the right panel. The data shown are representative of three independent experiments. Values represent the mean ± SEM. $^{*}P < 0.01$ and $^{***}P < 0.0001$ versus untreated controls at 18 hours by one-way ANOVA. (*C*) Instantaneous velocity of the leading front at different distances from the edge over time. (*D*) Velocity fields overlapped with phase-contrast images of migrating HNEC layers at the indicated time points. Magnified views of region delimited by white boxes in *A*. The arrow describes the angle of displacement, and the length is proportional to the magnitude. Scale bar: 50 μm. (*E*) The expression of pFAK-Y397, pFAK-Y925, and FAK was examined by Western blotting after IL-4 treatment with or without CMK for the indicated time periods. Relative densitometric values of either pFAK-Y397 or pFAK-Y925 to total FAK are shown in the bottom panel. Data are presented as mean ± SD ($n = 3$). $^{***}P < 0.0001$ versus untreated controls at 15 minutes post-stimulation by one-way ANOVA.

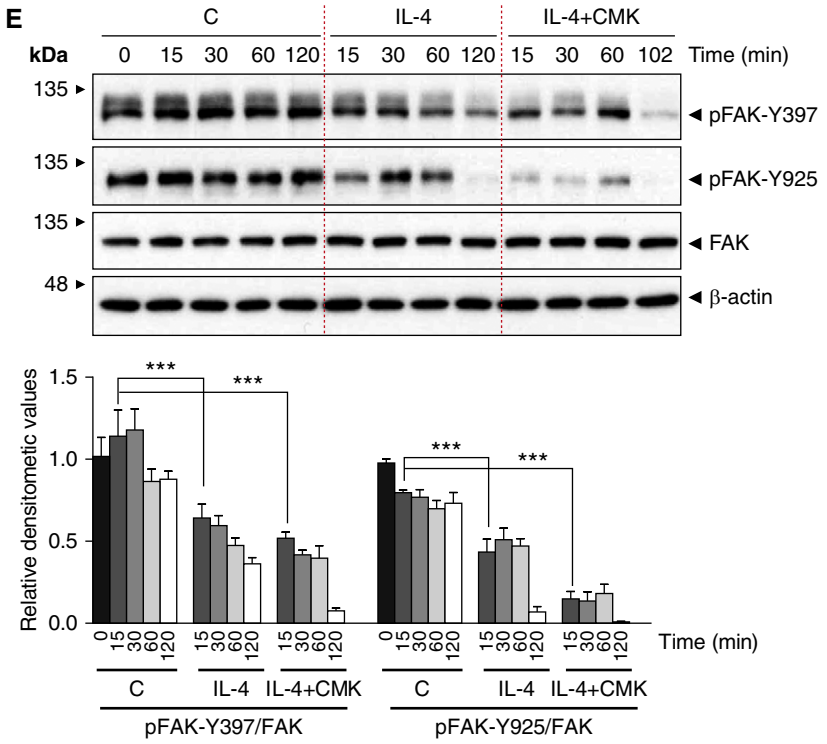


Figure 3. (Continued).

PC Inhibition Attenuates IL-4–induced Cell Migration by Suppressing Furin-mediated Pro–α_v-Integrin Activation

Interestingly, we observed that the combined treatment with IL-4 and 25 μM of the pan-PC inhibitor decanoyl-RVKR-chloromethylketone (CMK) (31) considerably decreased HNEC migration and FAK phosphorylation together with more sustained epithelial sheet contraction (Figure 3 and Movies E1–E3), compared with either no treatment or IL-4 treatment alone. The expression of $\alpha_v\beta_5$ and $\alpha_v\beta_6$ is persistently increased in undifferentiated basal epithelial cells during human airway epithelial wound repair (11, 32, 33). We also found that IL-4 upregulated the expression of α_v-, β_5-, and β_6-integrin subunits as well as the phosphorylation of FAK in HNECs (Figure E1A). Furthermore, immunofluorescence analyses revealed that the vast majority of cells expressing $\alpha_v\beta_5$ or $\alpha_v\beta_6$ in IL-4–stimulated HNECs were positive for BC marker keratin KRT5 (Figure E1B) (34). More importantly, α_v-integrin undergoes endoproteolytic cleavage by PCs to become biologically active (14). We previously showed that primary HNECs express two PCs, furin and PACE4, and that CMK reduces the expression of furin but not PACE4 (16, 17). To determine whether CMK is capable of inhibiting pro–α_v-integrin processing in HNECs, protein lysates isolated from HNECs treated with IL-4 in the presence or absence of CMK for 24 hours were subjected to Western blot analyses. Indeed, CMK strongly inhibited pro–α_v-integrin processing as well as furin expression (Figure 4A). To further investigate the role of furin in the processing of pro–α_v-integrin in HNECs, HNECs were transduced with lentivirus expressing either a scrambled shRNA (a negative control) or shRNAs targeting either furin or PACE4. The data showed that knockdown of furin but not PACE4 impaired pro–α_v-integrin processing (Figure 4B). These data suggest that CMK attenuates IL-4–induced HNEC migration, possibly by suppressing furin-mediated pro–α_v-integrin subunit processing and focal adhesion dynamics.

Integrins $\alpha_v\beta_5$ and $\alpha_v\beta_6$ Are Required for IL-4–induced Collective HNEC Migration via FAK Signaling Pathways

We next investigated whether IL-4 can induce collective cellular motion with dynamic cellular rearrangements in the well-differentiated HNEC layers, and if so, whether it can be inhibited by CMK or function-blocking antibodies specific for $\alpha_v\beta_5$ or $\alpha_v\beta_6$ (10 μg/ml). HNECs were treated with control mouse IgG, CMK, anti-$\alpha_v\beta_5$, or anti-$\alpha_v\beta_6$ in the presence of IL-4 in the basolateral compartment. The AP level of the HNEC layers was tracked by time-lapse video microscopy for 18 hours at 3-minute intervals, and a displacement field per unit time was calculated for successive phase-contrast images of HNECs over the last 3-hour period of the entire observation period using particle image velocimetry. Then we determined the spatiotemporal velocity distribution within the HNEC layers. A heat map showing the spatial distribution of velocity fields indicated that untreated controls displayed relatively small cellular motions and rare cellular rearrangements among neighboring cells (cold or blue regions in Figure 5A, first row, left panel, and Movie E4) together with low-velocity vectors (Figure 5A, middle panel) with velocity of 1.20 ± 0.67 μm h^{-1} (Figure 5B). In contrast, IL-4–stimulated HNEC layers exhibited a homogeneous distribution of clusters of high-velocity vectors (hot or red regions in Figure 5A, second row) with velocity of 1.97 ± 1.25 μm h^{-1} (Figure 5B) and dynamic swirl patterns with cooperative cellular rearrangements in an unjammed, fluid-like state (Movie E5). Notably, CMK suppressed IL-4–induced collective cell migration with significantly lower migration velocity of 1.47 ± 0.90 μm h^{-1} ($P < 0.0001$) (Figure 5A, third row, and Figure 5B, and Movie E6) compared with IL-4 alone. Interestingly, the HNEC layers treated with anti-$\alpha_v\beta_5$ and IL-4 showed that the heat map shifted closer to zero (cold or blue regions, Figure 5A, fourth rows), whereas the HNEC layers treated with anti-$\alpha_v\beta_6$ and IL-4 exhibited a heterogeneous distribution of clusters of velocity vectors (Figure 5A, fifth rows). Consistently, IL-4–induced HNEC migration was significantly inhibited by anti-$\alpha_v\beta_5$ (velocity = 1.06 ± 0.35 μm h^{-1}) and, to a lesser extent, with anti-$\alpha_v\beta_6$ (velocity = 1.44 ± 0.87 μm h^{-1}) (Figure 5B and Movies E7 and E8).

Furthermore, confocal microscopic analysis of actin distribution visualized with FITC-phalloidin at the BL level revealed that HNECs treated with anti-$\alpha_v\beta_5$ and IL-4 displayed cobblestone-like shapes similar to untreated controls, whereas HNECs treated with anti-$\alpha_v\beta_6$ and IL-4 displayed a mix of cobblestone and spindle morphologies

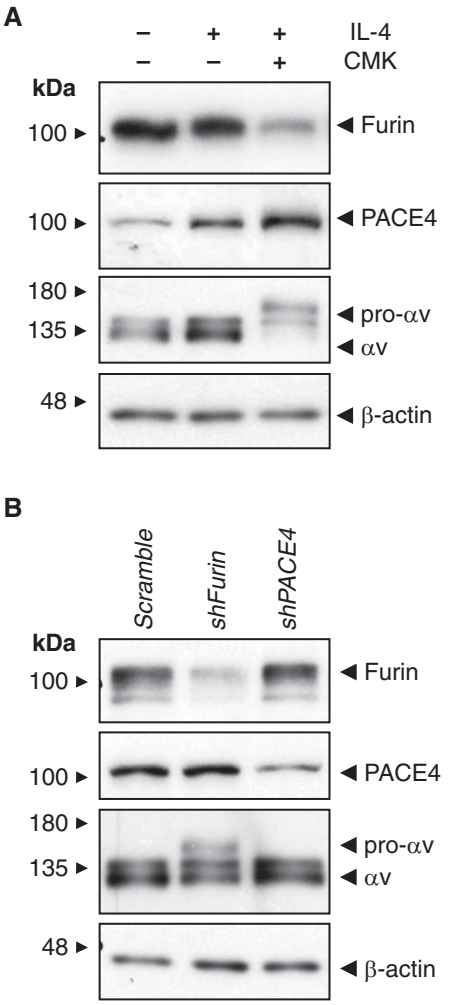


Figure 4. Proprotein convertase inhibition or furin knockdown suppresses pro-α_v-integrin processing. (*A*) Well-differentiated human nasal epithelial cells were cultured for 24 hours with IL-4 in the presence or absence of decanoyl-RVKR-CMK. Cell lysates were immunoblotted with antibodies to furin, paired basic amino acid–cleaving enzyme 4 (PACE4), and α_v-integrin. β-Actin was used as a loading control. (*B*) On air–liquid interface Day 0, human nasal epithelial cells were transduced with lentivirus expressing either a scrambled shRNA control (scramble) or shRNAs targeting furin or PACE4. Two days after transduction, protein concentrations of furin, PACE4, α_v-integrin, and β-actin were determined by Western blotting. The data shown are representative of three independent experiments.

(Figure 5A, right panels). This led us to speculate about the differences in the expression and distribution of $\alpha_v\beta_5$ and $\alpha_v\beta_6$ in the IL-4–stimulated HNEC layers. A histogram of the velocity distribution for each group also indicated that the proportion of slow-moving cells increased in HNECs treated with either CMK, anti-$\alpha_v\beta_5$, or anti-$\alpha_v\beta_6$ in the presence of IL-4, compared with IL-4 alone (Figure 5C). This experiment therefore suggests that $\alpha_v\beta_5$ and, to a lesser extent, $\alpha_v\beta_6$ are critically required for the IL-4–induced collective cell migration in the HNEC layers.

In Western blot analysis, we observed that the addition of CMK, anti-$\alpha_v\beta_5$, or anti-$\alpha_v\beta_6$ in the presence of IL-4 reduced the concentrations of pFAK-Y397 and pFAK-Y925 in HNECs, compared with IL-4 alone (Figure 5D), indicating that both $\alpha_v\beta_5$ and $\alpha_v\beta_6$ regulate the FAK activity in IL-4–stimulated HNECs. In addition, an ECM protein, periostin, which is known to alter the biomechanical properties of the ECM by collagen crosslinking and to interact with integrins, including $\alpha_v\beta_5$ (35, 36), was considerably upregulated in IL-4–stimulated HNECs (Figure 5D). To further test if periostin is involved in the IL-4–induced HNEC migration, HNECs were treated with antiperiostin (10 μg/ml) in the presence of IL-4, tracked by time-lapse video microscopy, and cell shape was determined by confocal microscopy of actin filaments stained with FITC-phalloidin (Figure E2). Both live-cell imaging and confocal microscopic analyses revealed that the addition of antiperiostin with IL-4 partially inhibited IL-4–induced HNEC migration, implying the existence of additional ligands such as vitronectin, collagen, and fibronectin (37). Surprisingly, IL-4–induced periostin expression was drastically decreased by anti-$\alpha_v\beta_5$ (Figure 5D), but not by anti-$\alpha_v\beta_6$, leading us to speculate that IL-4 promotes collective cellular motion in the HNEC layers, at least in part through interaction of periostin with $\alpha_v\beta_5$. We also observed that the addition of anti-$\alpha_v\beta_5$ with IL-4 led to near-complete loss of FAK phosphorylation, whereas the addition of anti-$\alpha_v\beta_6$ with IL-4 partially reduced FAK phosphorylation. Moreover, the addition of anti-$\alpha_v\beta_5$ with IL-4 induced the cleavage of caspase 3, an apoptosis maker, and the cleavage of PARP, a substrate for active caspase 3, whereas anti-$\alpha_v\beta_6$ had no effect (Figure E3). It is tempting to speculate that $\alpha_v\beta_5$ is enriched in BCs and that it is important in cell anchorage to the ECM as well as the immediate response to injury, whereas $\alpha_v\beta_6$ is expressed in distinct subpopulations of BCs and has a unique contribution to IL-4–induced collective HNEC migration. Taken together, these results strongly suggest that both $\alpha_v\beta_5$ and $\alpha_v\beta_6$ in BCs play a pivotal role in IL-4–induced collective HNEC migration through FAK signaling.

Expression and Distribution of $\alpha_v\beta_5$ and $\alpha_v\beta_6$ in the Nasal Epithelium of Patients with AR

We further elucidated the *in vivo* relevance of $\alpha_v\beta_5$ and $\alpha_v\beta_6$ in the processes of repair and regeneration after an injury. At steady state, KRT5 is expressed in most BCs, and KRT14 is expressed in a subpopulation of BCs, whereas both KRT5 and KRT14 are upregulated in the BC population during injury and repair (34). Therefore, by Western blotting, we determined the expression levels of β_5-integrin, β_6-integrin, KRT5, and KRT14 in the nasal epithelial brushings obtained from patients with AR and healthy control subjects (Figure 6A, upper panels). Interestingly, KRT5 and β_5-integrin were expressed in nasal brushing samples from both patients with AR and control subjects, whereas KRT14 and β_6-integrin were hardly detected in healthy control samples but were upregulated in AR patient samples. In addition, immunofluorescence analysis of the nasal epithelial brushings obtained from patients with AR showed that some of the cells expressing β_5- or β_6-integrin were positively stained for KRT14 (Figure 6A, lower panels). Furthermore, immunohistochemical analysis of the nasal mucosa obtained from four different patients with AR revealed that strong immunoreactivity for β_5-integrin was confined mostly to the BC layer in an area of injury as well as in the hyperplastic epithelium (Figure 6B, middle panels), whereas β_6-integrin immunoreactivity was presented in distinct subpopulations of epithelial cells (Figure 6B, right panels). Note that the injured area of epithelium that appears as relatively undifferentiated BCs without columnar cells showed strong immunohistochemical positivity for both β_5- and β_6-integrins (Figure 6B, arrowheads in second row). These results suggest that both β_5- and β_6-integrins are correlated with the processes of repair and regeneration that occur after damage of human nasal epithelium by AR.

Discussion

A positive correlation between prolonged or sustained cell migration and persistent TJ defects allows increased antigenic penetration

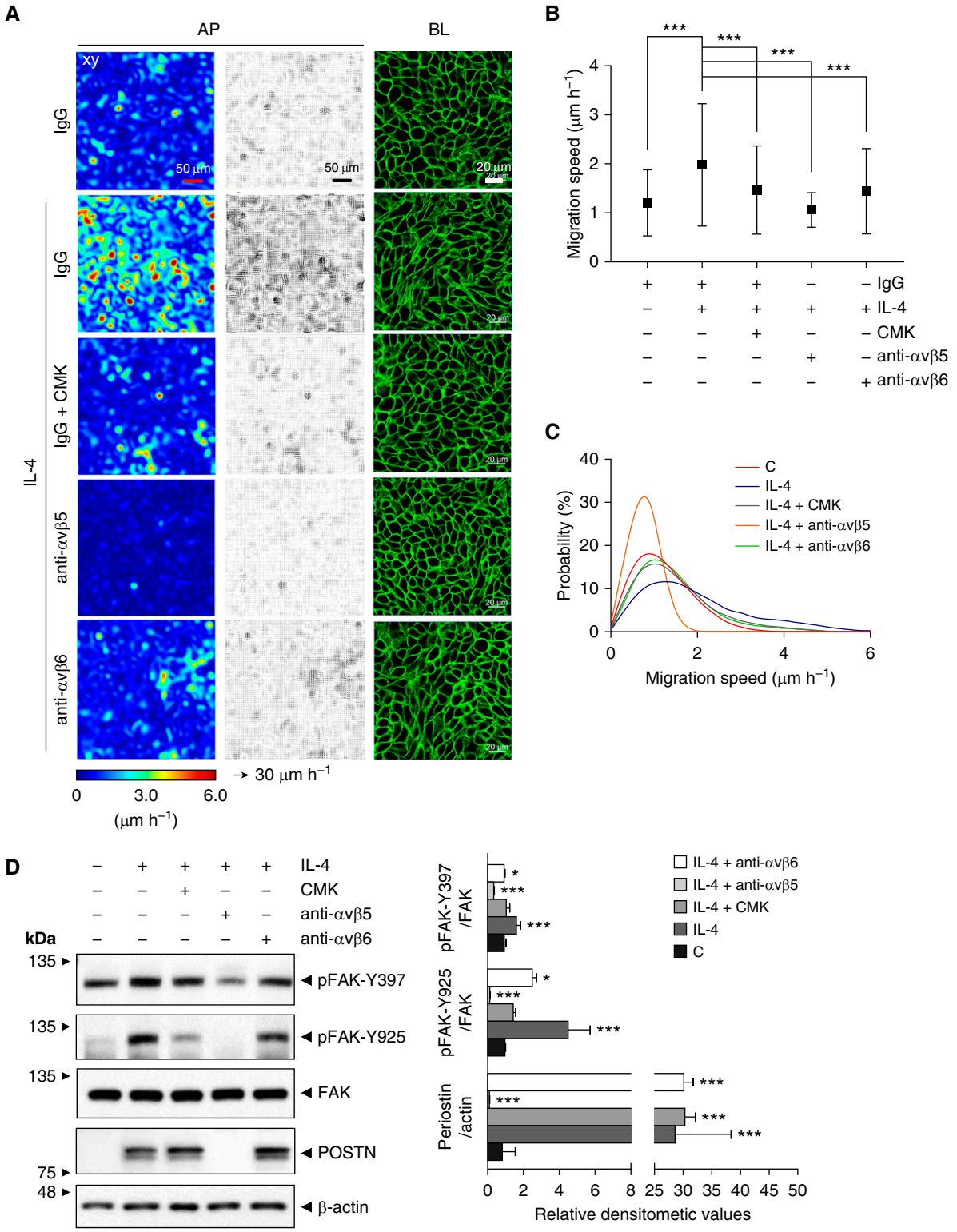


Figure 5. Integrins $\alpha_v\beta_5$ and $\alpha_v\beta_6$ are involved in IL-4–induced collective HNEC migration through activation of FAK signaling. Well-differentiated HNECs were treated with IgG control (10 μg/ml), decanoyl-RVKR-CMK (25 μM), anti-$\alpha_v\beta_5$ (10 μg/ml), or anti-$\alpha_v\beta_6$ (10 μg/ml) in the presence or absence IL-4. The AP level of the HNEC layers was tracked by time-lapse video microscopy for 18 hours at 3-minute intervals. Images of moving HNECs were taken over the last 3-hour period, then we calculated a displacement field per unit time using particle image velocimetry and determined the spatiotemporal velocity distribution within the HNEC layers. Mouse IgG was used as a control for anti-$\alpha_v\beta_5$ and anti-$\alpha_v\beta_6$. (*A*) Heat map showing spatial distribution of velocity fields at a given instant (left panels) and quiver plots displaying speed and direction as arrows (black lines in middle panels). Scale bars: 50 μm.

and contact between ligand–receptor pairs. These pairs are segregated in different domains under steady-state conditions, finally leading to exacerbated airway inflammation and remodeling by sustained activation of signaling pathways that affect the expression of specific genes and the production of ECM molecules (5, 7, 18). Allergens and Th2 cytokines appear to disrupt epithelial barrier integrity through decreased TJ protein expression, increased epithelial permeability, and decreased cell–ECM interactions in the airway epithelium, all of which are required for cell migration initiation (18, 19, 38). Our findings demonstrate that $\alpha_v\beta_5$ and $\alpha_v\beta_6$ integrins serve as critical mechanoreceptors that allow HNECs to detect and respond to biomechanical changes in the ECM after IL-4 stimulation, leading to collective cell migration through FAK-mediated signaling pathways.

Collective cell migration is the coordinated movement of a large cluster of cells by maintaining strong E-cadherin–mediated cell–cell adhesion and by altering actin cytoskeleton organization, TJ function, and cellular polarity (6, 7). Because epithelial cells are mechanically coupled to the actin cytoskeleton at E-cadherin–based AJs and at integrin-mediated focal contacts (6–8, 27, 28), E-cadherin–mediated cell–cell and integrin-based cell–ECM interactions are crucial for individual cells to respond to changes in their environments via actin-myosin contractility–driven contractile tension and cross-talk of these two adhesive types, as well as tissue architecture maintenance (28). Interestingly, our data show that IL-4 induces E-cadherin cleavage and asymmetric E-cadherin distribution in HNECs, as well as the formation of a refined boundary between two cell clusters by their affinities in a confluent layer of well-differentiated HNECs. Proteolytic cleavage of E-cadherin ectodomains plays an important role in a dynamic process that includes cell migration, proliferation, and survival under both physiological and pathological conditions (39). In the epithelial monolayers, ADAM10 (a disintegrin and metalloproteinase domain containing protein 10)-mediated E-cadherin cleavage at the interfaces between cells through Eph/ephrin signaling mediates the separation of different cell clusters by their affinities, which is essential for the regulation of cell migration and tissue assembly (40). Consistent with this concept, the present study revealed that IL-4 induces cell shape changes driven by actin cytoskeleton reorganization and phenotypic EMT-like changes in the HNEC layers. Cell shape changes systematically drive cellular rearrangements and motility, leading to the transition from a jammed, solid-like state to an unjammed, fluid-like state (23, 24). Indeed, The AP confocal plane of the untreated control layers exhibited a relatively ordered polygonal packing pattern with different numbers of neighboring cells, whereas the AP plane of the IL-4–stimulated layers showed more irregular and elongated shapes. The vertex model links cell mechanics to cell shape and cell motility in a two-dimensional confluent layer that is represented as a polygonal tiling of the plane with no gaps or overlaps (22, 24). In this model, the AP cell shapes are determined by mechanical forces generated by cell area elasticity, line tension along AP junctions, and contractility of the actin-myosin ring (22). These physical effects generate an effective cell shape index p_0 (ratio of the cell perimeter to the square root of the cell area): The preferred area is determined by cell height and cell volume, and the cell perimeter is determined by the competition between cell–cell adhesion and contractile cortical tension within the layer plane (22). Of note, the perimeter of the cell–cell junction is increased by reducing actin-myosin contractility or increasing cell–cell adhesion, and a rigidity transition of the cellular collective occurs at a critical value of $p_0 \approx 3.81$ (p_0^*) (23, 24). Therefore, if $p_0 < p_0^*$, the cell layer becomes jammed, whereas if $p_0 > p_0^*$, the cell layer becomes unjammed (24). Our analysis revealed that the median of p_0 for untreated controls was 3.80, whereas the median of p_0 for IL-4–stimulated cells is 4.56, strongly suggesting that IL-4 induces the jammed-to-unjammed transition in the well-differentiated HNEC layers. We also observed that the BL confocal plane of the IL-4–stimulated HNEC layers displayed morphological alteration of BCs from their typical cobblestone shape to a spindle shape, as well as actin cytoskeleton reorganization with actin stress fiber induction, indicating that BCs undergo EMT-like changes. Taken together, this suggests that IL-4–stimulated HNECs form a tightly packed cluster with equivalent strength of E-cadherin–mediated adhesions that migrates collectively. The mechanism underlying the separation of different cell clusters in the IL-4–stimulated HNEC layers will be addressed in future experiments. Surprisingly, we observed that IL-4 induces initial transient contraction of the HNEC layers from the leading front after wounding and also that it inhibits the phosphorylation of FAK at Tyr397 and Tyr925, which is required for the integrin-mediated cell attachment to the ECM and the focal adhesion turnover (9), in the early phase of wound repair. We therefore speculate that IL-4 induces initial transient contraction of the wounded epithelial sheet, possibly by reducing integrin-based cell–ECM adhesions and FAK phosphorylation. Given that IL-4 decreases epithelial cell–ECM interactions (20), that AP junctions with neighboring cells are under tension generated by actin-myosin contractility at cell boundaries (22), and that release of tension exerted by cells on the ECM after actin cytoskeleton collapse and loss of cell surface triggers transient cell hypercontraction (29, 30), it is possible that transient cellular contractility and mechanical stresses arising from an IL-4–induced imbalance of E-cadherin–mediated cell–cell and integrin-based cell–ECM interactions may trigger the initiation of collective cellular motion to maintain minimal local intercellular shear stress by pushing and pulling from the surrounding cells in a confluent HNEC layer (41, 42).

Cell migration requires dynamic interactions between cells and the ECM via integrins linked to the actin cytoskeleton (8).

Figure 5. (Continued). Confocal immunofluorescence of actin stained with phalloidin in HNECs treated with IL-4 for 24 hours. Confocal *x–y* sections at the basal (BL) level of the HNEC layers are shown (right panels). Scale bars: 20 μm. (*B*) Average HNEC migration speed. Values represent the mean ± SD. ***$P < 0.0001$ by Student's *t* test. (*C*) Histogram of the velocity distribution for each group. Magnitude of the resulting velocity vectors was used to characterize the velocity histogram of each group. The area of each histogram was normalized to the total number of velocity vectors in each group. (*D*) HNECs were treated with either CMK, anti-$\alpha_v\beta_5$, or anti-$\alpha_v\beta_6$ in the presence of IL-4 for 24 hours. The expression of pFAK-Y397, pFAK-Y925, FAK, and periostin were examined by Western blotting. Bottom panel shows densitometric data from the blots ($n = 3$). Samples were normalized to β-actin content, and results are presented as mean ± SD. *$P < 0.01$ and ***$P < 0.0001$ versus untreated controls by one-way ANOVA.

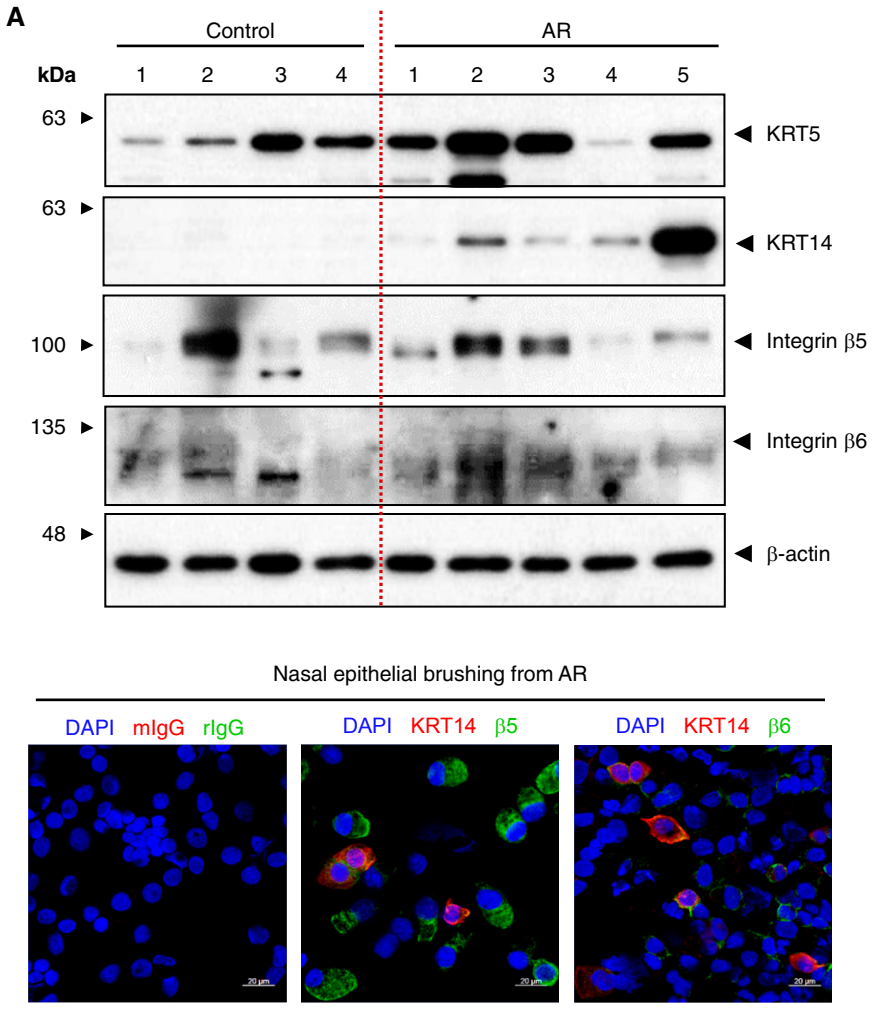


Figure 6. Expression and distribution of β_5- and β_6-integrins in the nasal epithelium of patients with allergic rhinitis (AR). (*A*) Nasal epithelial brushings obtained from patients with AR and healthy control subjects were used to determine the expression of keratin 5 (KRT5), KRT14, and β_5- and β_6-integrins by Western blot analysis. β-Actin was used as a loading control (upper panels). Representative immunofluorescence image of cytopreparations generated from the nasal epithelial brushings obtained from patients with AR stained for control IgG (lower panels, left), anti-KRT14 and anti-β5 (lower panels, middle), and anti-KRT14 and anti-β6 antibodies (lower panels, right). Scale bars: 20 μm. (*B*) Immunohistochemical analysis was performed using paraffin-embedded tissue sections (4 μm) of nasal mucosa specimens obtained from four different patients with AR and a healthy control subject. Sections were immunostained by either β_5-integrin (middle panels) or β_6-integrin (right panels) antibodies. Rabbit IgG was used as a staining negative control (left panels). Arrowheads represent areas of damaged epithelium, which appear as relatively undifferentiated basal cells without columnar cells. Scale bars: 20 μm. m = mouse; r = rabbit.

During human airway epithelial wound repair, epithelial cells exhibit a persistent upregulation of $\alpha_v\beta_5$ and $\alpha_v\beta_6$, a transient upregulation of $\alpha_5\beta_1$, and a redistribution of $\alpha_6\beta_4$ (11). It has been reported that α_v-coupled β-integrins (β_1-, β_3-, β_5-, and β_6-integrins) positively control FAK expression and activation (12, 13). We also found that the expression of α_v-, β_5-, and β_6-integrins and pFAK was increased in HNECs in response to basolateral IL-4 stimulation (Figure E1). More importantly, α_v-integrin undergoes endoproteolytic cleavage by PCs to become biologically active (14). We previously reported that primary HNECs cultured at the ALI express two PC family members, furin and PACE4 (16, 17). Not surprisingly, the addition of CMK with IL-4 considerably decreased collective HNEC migration and decreased pro–α_v-integrin processing compared with IL-4 treatment alone. In addition, *Furin* knockdown, but not *PACE4* knockdown, inhibited pro–α_v-integrin processing. Moreover, the addition of CMK with IL-4 induced more sustained HNEC layer contraction than IL-4 treatment alone. Taking these data together, we speculate that CMK inhibits IL-4–induced collective HNEC migration, possibly owing to inhibition of the turnover of focal contacts by suppressing furin-mediated pro–α_v-integrin processing. However, we cannot exclude the possibility that the processing of other furin substrates, pro-α_5 and pro-α_6 (43), that show alteration of expression and distribution during human airway epithelial wound repair (11) might directly or indirectly contribute to increased HNEC migration by IL-4 stimulation.

In further support of the involvement of α_v-integrin in collective HNEC migration, live-cell imaging revealed that IL-4 induced collective cell migration with dynamic cellular rearrangements in the HNEC layers and that the effect of IL-4 on collective cell migration in the well-differentiated HNEC layers was reversed after basolateral addition of function-blocking antibodies for $\alpha_v\beta_5$ or $\alpha_v\beta_6$. Similar results were observed with the addition of anti-$\alpha_v\beta_5$ or anti-$\alpha_v\beta_6$ on Day 2 of ALI culture, long before the appearance of differentiated cells (Figure E4), suggesting that cell–ECM interactions mediated by $\alpha_v\beta_5$ and $\alpha_v\beta_6$ expressed on BCs play an important role in IL-4–stimulated collective HNEC migration. Consistent with these observations, anti-$\alpha_v\beta_5$ and anti-$\alpha_v\beta_6$ significantly reduced the FAK phosphorylation in IL-4–stimulated HNECs, implying that both integrins have major roles in IL-4–induced collective HNEC migration through an FAK signaling pathway. Most ECM proteins can be recognized by different integrins in response to injury and inflammation (44). Periostin has been demonstrated to promote allergic inflammation in response to Th2 cytokines and to provide signals to initiate a variety of biologic effects, including cell migration and tissue remodeling (35, 36, 45). It can alter the biomechanical properties of the ECM by collagen crosslinking and interact with multiple integrins, including $\alpha_v\beta_3$, $\alpha_v\beta_5$, and $\alpha_6\beta_4$ (35, 46). Our data demonstrate that periostin is upregulated in IL-4–stimulated HNECs and that the addition of antiperiostin partially reduces IL-4–induced collective HNEC migration, implying the existence of additional ligands such as vitronectin, collagen, and

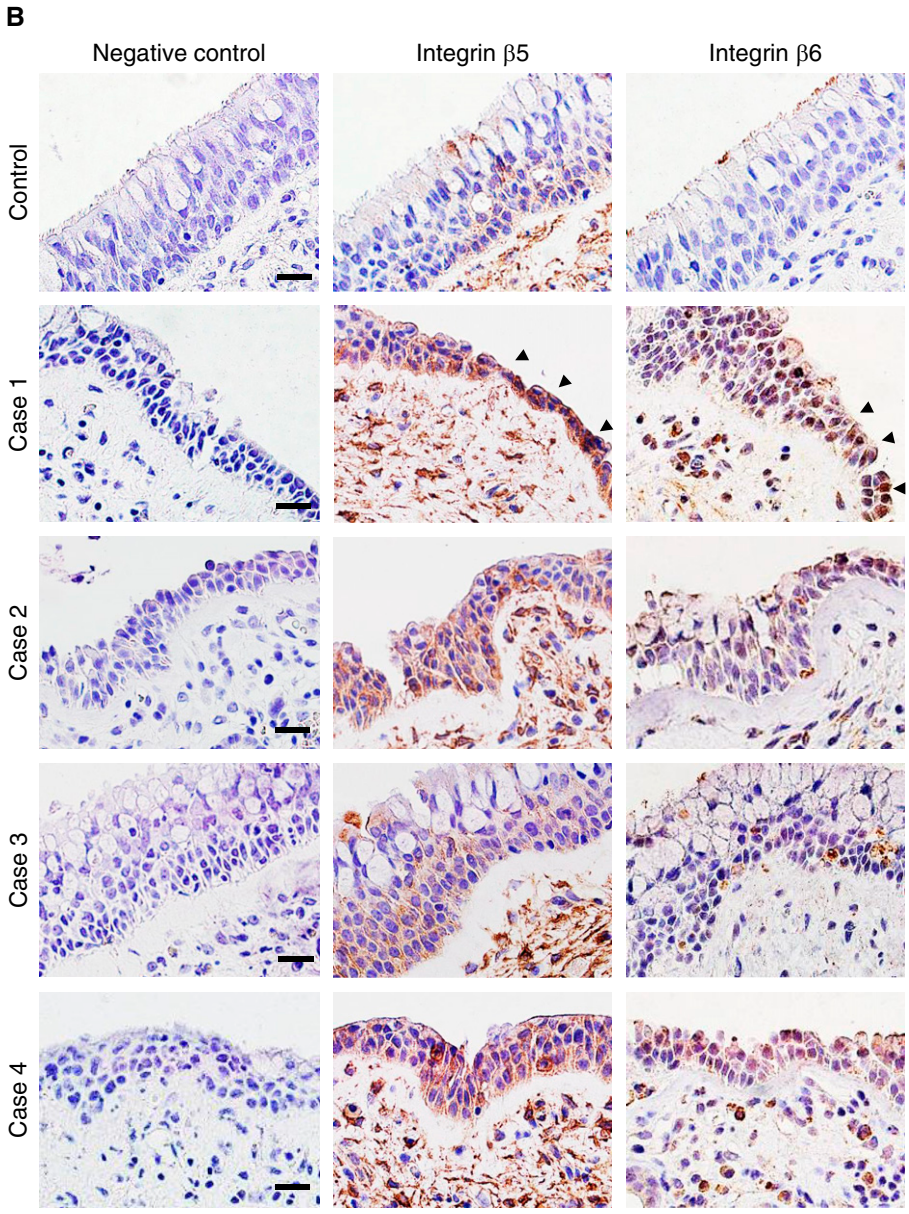


Figure 6. (Continued).

fibronectin (37). In addition, periostin expression was completely reversed by anti-$\alpha_v\beta_5$, but not by anti-$\alpha_v\beta_6$, leading us to speculate that IL-4 promotes collective cellular motion in the HNEC layers, at least in part through interaction of periostin with $\alpha_v\beta_5$. Interestingly, the efficacy of anti-$\alpha_v\beta_5$ in inhibiting IL-4–induced collective cell migration and FAK phosphorylation was much higher than that of anti-$\alpha_v\beta_6$. In addition, HNECs treated with anti-$\alpha_v\beta_5$ and IL-4 showed cobblestone-like morphology, whereas anti-$\alpha_v\beta_6$ and IL-4 treatment promoted a mix of cobblestone- or spindle-shaped morphologies. Given that $\alpha_v\beta_5$ is constitutively expressed in the undifferentiated nasal and bronchial airway epithelial cells (32) and that FAK can also contribute to survival signaling that is required for ECM-dependent survival (47), and considering the induction of anchorage loss-detachment cell death of HNECs by the addition of anti-$\alpha_v\beta_5$ but not anti-$\alpha_v\beta_6$ demonstrated in the present study (Figure E3), it is possible that $\alpha_v\beta_5$ enriched in BCs is important in cell anchorage to the ECM under steady-state conditions as well as in the immediate response to injury. In contrast, $\alpha_v\beta_6$ expressed in distinct subpopulations of BCs by IL-4 stimulation has a unique contribution to collective HNEC migration. However, this has to be clarified in future experiments.

We found that $\alpha_v\beta_5$ and $\alpha_v\beta_6$ are also of high relevance for the process in epithelial repair and regeneration after an injury *in vivo*. It has been reported that at steady state, KRT5 is expressed in most BCs and KRT14 is expressed in a subpopulation of BCs, whereas both KRT5 and KRT14 are upregulated in the BC population during injury and repair (34). Our analysis revealed that KRT5 and β_5-integrin were expressed in nasal brushing samples from both patients with AR and healthy control subjects, whereas KRT14 and β_6-integrin were hardly detected in healthy control samples but were upregulated in AR patient samples. In addition, our immunostaining of the nasal epithelium obtained from patients with AR demonstrated that β_5-integrin is expressed in most BCs, whereas β_6-integrin is expressed in distinct subpopulations of BCs. Moreover, a strong immunoreactivity for both β_5- and β_6-integrins appeared in areas of damaged epithelium. Collectively, these data suggest that $\alpha_v\beta_5$ and $\alpha_v\beta_6$ are correlated with the process of epithelial repair and regeneration that occurs after damage of human nasal epithelium with AR.

In summary, our findings demonstrate that in well-differentiated HNECs, IL-4 induces transient contraction, TJ disruption, cleavage, and asymmetric distribution of E-cadherin, cell shape changes, and actin cytoskeleton reorganization, leading to collective cell migration in the HNEC layers. The effect of IL-4 on collective HNEC migration is reversed by pharmacologic and genetic inhibition of the α_v-integrin–activating enzyme furin and function-blocking antibodies for $\alpha_v\beta_5$, $\alpha_v\beta_6$, or periostin. Selective targeting of either $\alpha_v\beta_5$ or $\alpha_v\beta_6$ may be a useful strategy for preventing progression and exacerbation of chronic allergic airway disease at early stages. ■

Author disclosures are available with the text of this article at www.atsjournals.org.

Acknowledgment: The authors thank Dr. Jin-Ah Park for the discussion for the initiation of this project.

References

1. Schleimer RP, Berdnikovs S. Etiology of epithelial barrier dysfunction in patients with type 2 inflammatory diseases. *J Allergy Clin Immunol* 2017;139:1752–1761.
2. Lloyd CM, Robinson DS. Allergen-induced airway remodelling. *Eur Respir J* 2007;29:1020–1032.
3. Puchelle E, Zahm JM, Tournier JM, Coraux C. Airway epithelial repair, regeneration, and remodeling after injury in chronic obstructive pulmonary disease. *Proc Am Thorac Soc* 2006;3: 726–733.
4. Gibson MC, Perrimon N. Apicobasal polarization: epithelial form and function. *Curr Opin Cell Biol* 2003;15:747–752.
5. Vermeer PD, Einwalter LA, Moninger TO, Rokhlina T, Kern JA, Zabner J, *et al*. Segregation of receptor and ligand regulates activation of epithelial growth factor receptor. *Nature* 2003;422: 322–326.
6. Sadati M, Taheri Qazvini N, Krishnan R, Park CY, Fredberg JJ. Collective migration and cell jamming. *Differentiation* 2013;86:121–125.
7. Notbohm J, Banerjee S, Utuje KJC, Gweon B, Jang H, Park Y, *et al*. Cellular contraction and polarization drive collective cellular motion. *Biophys J* 2016;110:2729–2738.
8. Hu YL, Lu S, Szeto KW, Sun J, Wang Y, Lasheras JC, *et al*. FAK and paxillin dynamics at focal adhesions in the protrusions of migrating cells. *Sci Rep* 2014;4:6024.
9. Mitra SK, Hanson DA, Schlaepfer DD. Focal adhesion kinase: in command and control of cell motility. *Nat Rev Mol Cell Biol* 2005;6: 56–68.
10. Teoh CM, Tan SSL, Tran T. Integrins as therapeutic targets for respiratory diseases. *Curr Mol Med* 2015;15:714–734.
11. Pilewski JM, Latoche JD, Arcasoy SM, Albelda SM. Expression of integrin cell adhesion receptors during human airway epithelial repair in vivo. *Am J Physiol* 1997;273:L256–L263.
12. Mitra SK, Schlaepfer DD. Integrin-regulated FAK-Src signaling in normal and cancer cells. *Curr Opin Cell Biol* 2006;18: 516–523.
13. Duperret EK, Dahal A, Ridky TW. Focal-adhesion-independent integrin-αv regulation of FAK and c-Myc is necessary for 3D skin formation and tumor invasion. *J Cell Sci* 2015;128: 3997–4013.
14. Shiryaev SA, Chernov AV, Golubkov VS, Thomsen ER, Chudin E, Chee MS, *et al*. High-resolution analysis and functional mapping of cleavage sites and substrate proteins of furin in the human proteome. *PLoS One* 2013;8:e54290.
15. Seidah NG, Prat A. The biology and therapeutic targeting of the proprotein convertases. *Nat Rev Drug Discov* 2012;11: 367–383.
16. Lee SN, Choi IS, Kim HJ, Yang EJ, Min HJ, Yoon JH. Proprotein convertase inhibition promotes ciliated cell differentiation – a potential mechanism for the inhibition of Notch1 signalling by decanoyl-RVKR-chloromethylketone. *J Tissue Eng Regen Med* 2017;11:2667–2680.
17. Lee SN, Lee DH, Lee MG, Yoon JH. Proprotein convertase 5/6a is associated with bone morphogenetic protein-2-induced squamous cell differentiation. *Am J Respir Cell Mol Biol* 2015;52: 749–761.
18. Georas SN, Rezaee F. Epithelial barrier function: at the front line of asthma immunology and allergic airway inflammation. *J Allergy Clin Immunol* 2014;134:509–520.
19. Soyka MB, Wawrzyniak P, Eiwegger T, Holzmann D, Treis A, Wanke K, *et al*. Defective epithelial barrier in chronic rhinosinusitis: the regulation of tight junctions by IFN-γ and IL-4. *J Allergy Clin Immunol* 2012;130:1087–1096.e10.
20. Ramirez-Icaza G, Mohammed KA, Nasreen N, Van Horn RD, Hardwick JA, Sanders KL, *et al*. Th2 cytokines IL-4 and IL-13 downregulate paxillin expression in bronchial airway epithelial cells. *J Clin Immunol* 2004;24:426–434.
21. White SR, Martin LD, Abe MK, Marroquin BA, Stern R, Fu X. Insulin receptor substrate-1/2 mediates IL-4-induced migration of human airway epithelial cells. *Am J Physiol Lung Cell Mol Physiol* 2009;297: L164–L173.
22. Aegerter-Wilmsen T, Smith AC, Christen AJ, Aegerter CM, Hafen E, Basler K. Exploring the effects of mechanical feedback on epithelial topology. *Development* 2010;137:499–506.
23. Park JA, Kim JH, Bi D, Mitchel JA, Qazvini NT, Tantisira K, *et al*. Unjamming and cell shape in the asthmatic airway epithelium. *Nat Mater* 2015;14:1040–1048.
24. Bi D, Yang X, Marchetti MC, Manning ML. Motility-driven glass and jamming transitions in biological tissues. *Phys Rev X* 2016;6: 021011.
25. Yoon JH, Kim KS, Kim SS, Lee JG, Park IY. Secretory differentiation of serially passaged normal human nasal epithelial cells by retinoic acid: expression of mucin and lysozyme. *Ann Otol Rhinol Laryngol* 2000;109:594–601.
26. Shin HW, Cho K, Kim DW, Han DH, Khalmuratova R, Kim SW, *et al*. Hypoxia-inducible factor 1 mediates nasal polypogenesis by inducing epithelial-to-mesenchymal transition. *Am J Respir Crit Care Med* 2012;185:944–954.
27. Wang Y, Wang X. Integrins outside focal adhesions transmit tensions during stable cell adhesion. *Sci Rep* 2016;6: 36959.
28. Weber GF, Bjerke MA, DeSimone DW. Integrins and cadherins join forces to form adhesive networks. *J Cell Sci* 2011;124: 1183–1193.
29. Sen S, Kumar S. Cell-matrix de-adhesion dynamics reflect contractile mechanics. *Cell Mol Bioeng* 2009;2:218–230.
30. Vasiliev JM, Omelchenko T, Gelfand IM, Feder HH, Bonder EM. Rho overexpression leads to mitosis-associated detachment of cells from epithelial sheets: a link to the mechanism of cancer dissemination. *Proc Natl Acad Sci USA* 2004;101: 12526–12530.
31. Hallenberger S, Bosch V, Angliker H, Shaw E, Klenk HD, Garten W. Inhibition of furin-mediated cleavage activation of HIV-1 glycoprotein gp160. *Nature* 1992;360:358–361.
32. McDougall CM, Blaylock MG, Douglas JG, Brooker RJ, Helms PJ, Walsh GM. Nasal epithelial cells as surrogates for bronchial epithelial cells in airway inflammation studies. *Am J Respir Cell Mol Biol* 2008; 39:560–568.
33. Fernandes DJ, Bonacci JV, Stewart AG. Extracellular matrix, integrins, and mesenchymal cell function in the airways. *Curr Drug Targets* 2006;7:567–577.
34. Rock JR, Randell SH, Hogan BLM. Airway basal stem cells: a perspective on their roles in epithelial homeostasis and remodeling. *Dis Model Mech* 2010;3:545–556.
35. Sidhu SS, Yuan S, Innes AL, Kerr S, Woodruff PG, Hou L, *et al*. Roles of epithelial cell-derived periostin in TGF-β activation, collagen production, and collagen gel elasticity in asthma. *Proc Natl Acad Sci USA* 2010;107:14170–14175.
36. Ghatak S, Misra S, Norris RA, Moreno-Rodriguez RA, Hoffman S, Levine RA, *et al*. Periostin induces intracellular cross-talk between kinases and hyaluronan in atrioventricular valvulogenesis. *J Biol Chem* 2014;289:8545–8561.
37. Cirulli V, Beattie GM, Klier G, Ellisman M, Ricordi C, Quaranta V, *et al*. Expression and function of $\alpha_v\beta_3$ and $\alpha_v\beta_5$ integrins in the developing pancreas: roles in the adhesion and migration of putative endocrine progenitor cells. *J Cell Biol* 2000;150: 1445–1460.
38. Steelant B, Farré R, Wawrzyniak P, Belmans J, Dekimpe E, Vanheel H, *et al*. Impaired barrier function in patients with house dust mite-induced allergic rhinitis is accompanied by decreased occludin and zonula occludens-1 expression. *J Allergy Clin Immunol* 2016;137: 1043–1053.e5.
39. Maretzky T, Reiss K, Ludwig A, Buchholz J, Scholz F, Proksch E, *et al*. ADAM10 mediates E-cadherin shedding and regulates epithelial cell-cell adhesion, migration, and β-catenin translocation. *Proc Natl Acad Sci USA* 2005;102:9182–9187.
40. Solanas G, Cortina C, Sevillano M, Batlle E. Cleavage of E-cadherin by ADAM10 mediates epithelial cell sorting downstream of EphB signalling. *Nat Cell Biol* 2011;13:1100–1107.
41. Tambe DT, Hardin CC, Angelini TE, Rajendran K, Park CY, Serra-Picamal X, *et al*. Collective cell guidance by cooperative intercellular forces. *Nat Mater* 2011;10:469–475.

42. Köpf MH. Collective cell migration induced by mechanical stress and substrate adhesiveness. *Phys Rev E Stat Nonlin Soft Matter Phys* 2015;91:012712.
43. Lissitzky JC, Luis J, Munzer JS, Benjannet S, Parat F, Chrétien M, *et al*. Endoproteolytic processing of integrin pro-α subunits involves the redundant function of furin and proprotein convertase (PC) 5A, but not paired basic amino acid converting enzyme (PACE) 4, PC5B or PC7. *Biochem J* 2000;346:133–138.
44. Wright DB, Meurs H, Dekkers BGJ. Integrins: therapeutic targets in airway hyperresponsiveness and remodelling? *Trends Pharmacol Sci* 2014;35:567–574.
45. Masuoka M, Shiraishi H, Ohta S, Suzuki S, Arima K, Aoki S, *et al*. Periostin promotes chronic allergic inflammation in response to Th2 cytokines. *J Clin Invest* 2012;122:2590–2600.
46. Gillan L, Matei D, Fishman DA, Gerbin CS, Karlan BY, Chang DD. Periostin secreted by epithelial ovarian carcinoma is a ligand for $\alpha_V\beta_3$ and $\alpha_V\beta_5$ integrins and promotes cell motility. *Cancer Res* 2002;62: 5358–5364.
47. Zouq NK, Keeble JA, Lindsay J, Valentijn AJ, Zhang L, Mills D, *et al*. FAK engages multiple pathways to maintain survival of fibroblasts and epithelia: differential roles for paxillin and p130Cas. *J Cell Sci* 2009;122:357–367.

Title: Integrins αvβ5 and αvβ6 mediate IL-4-induced collective migration in human airway epithelial cells

Authors: Sang-Nam Lee, Ji-Suk Ahn, Seong Gyu Lee , Hyung-S uk Lee,
Augustine M. K. Choi, and Joo-Heon Yoon

ONLINE DATA SUPPLEMENT

Supplementary information (SI)

Materials and Methods

Antibodies and reagents – Mouse monoclonal anti-furin, mouse monoclonal anti-αv integrin, rabbit polyclonal anti-β6 integrin, normal mouse IgG, and mouse monoclonal anti-β-actin were purchased from Santa Cruz Biotechnology (Santa Cruz, CA). Mouse monoclonal anti-E-cadherin was obtained from BD Biosciences (San Jose, CA). Rabbit monoclonal anti-PACE4, rabbit polyclonal anti-β5 integrin, rabbit monoclonal anti-FAK, rabbit monoclonal anti-FAK (phosphor Y397 & Y925), goat polyclonal anti-periostin, mouse monoclonal anti-KRT5, rabbit polyclonal anti-KRT5, mouse monoclonal anti-KRT14, and rabbit polyclonal anti-KRT14 were obtained from Abcam (Cambridge, UK). Rabbit polyclonal anti-ZO-1 and mouse monoclonal anti-occludin were purchased from Thermo Scientific (Fremont, CA). Rabbit monoclonal anti-p-ERK, rabbit monoclonal anti-ERK, rabbit monoclonal anti-caspase-3, rabbit monoclonal anti-PARP, and rabbit monoclonal anti-vimentin were obtained from Cell Signaling (Beverly, MA). Mouse monoclonal anti-αvβ5 integrin, mouse monoclonal anti-αvβ6 integrin, and mouse monoclonal anti-α-SMA were purchased from Millipore (Temecula, CA). Decanoyl-RVKR-chloromethylketone (CMK) was obtained from Bachem (Bubendorf, Switzerland). FITC-labeled phalloidin and non-enzymatic cell dissociation solution were purchased from Sigma-Aldrich (St Louis, MO).

Cell culture – Human nasal epithelial cells (HNECs) were isolated from nasal polyps obtained from patients with chronic rhinosinusitis who had no clinical history of asthma, aspirin sensitivity, or cystic fibrosis. The air–liquid interface (ALI) culture system was used for HNECs, as previously described (Yoon et al., 1999). Briefly, passage-2 HNECs were seeded at a density of 2×10^5 cells/cm^2 on a 12 mm, 0.45 μm pore transwell-clear culture insert (Costar Co, Cambridge, MA, USA). Cells were cultured in a 1:1 mixture of BEGM and DMEM (Lonza, Basel, Switzerland), supplemented with growth factors according to the manufacturer's instructions: hydrocortisone (0.5 μg/ml), insulin (5 μg/ml), transferrin (10 μg/ml), epinephrine (0.5 μg/ml), triiodothyronine (6.5 μg/ml), gentamicin (50 μg/ml), amphotericin-B (50 μg/ml), retinoic acid (15 ng/ml), bovine pituitary extract (50 μg/ml), bovine serum albumin (1.5 μg/ml), and epidermal growth factor (0.5 ng/ml). As soon as the cells reached confluence, the apical surfaces of the cells were exposed to air (ALI). The ALI medium was added to the basolateral chamber every other day for 2 wk. IL-4 (5 ng/ml or 0-20 ng/mL) was added to the basolateral chamber at ALI day 14 for 24 h. In some experiments, cells were pretreated with, CMK (25 μM), or function-blocking antibodies (10 μg/ml) for 1 h, followed by IL-4 stimulation with the respective substances for an additional 24 h. Normal mouse IgG was used as a control of function-blocking antibodies. All experiments were carried out at least in duplicate on three separate stably transfected populations.

Western blotting – Superficial nasal mucosal cells were collected by brushing at the middle portion of the inferior turbinate using a soft sterile brush (Medical Packaging Camarillo, CA). Brush was gently spun and then immediately immersed and transferred to transfer media (Dulbecco's Modified Eagle's Medium: HAM's F12K medium + 1% Penicillin/Streptomycin) in 15-mL conical tubes. After vortexing of the conical tubes, tips were gently removed, tubes were centrifuged at 1,000 rpm, 4℃ for 5 minutes, and the supernatant was carefully aspirated. Nasal brush biopsies and HNE cells were homogenized in cell lysis buffer (Invitrogen, Camarillo, CA) containing 1 mM phenylmethylsulfonyl fluoride (PMSF) and the Halt protease and phosphatase inhibitor cocktail (Thermo Scientific, Rockford, IL) on ice. Samples were subjected to electrophoresis on either 8% or 12% SDS-PAGE gels, followed by western blotting using the appropriate antisera. Proteins were transferred from gels to PVDF membranes and the membranes was preincubated in 5% nonfat milk in Tris-buffered saline (50 mM Tris-Cl, pH 7.5, 150 mM NaCl) containing 0.5% Tween 20 (TTBS) for 1 h at room temperature prior to incubation overnight at 4℃ with antiserum diluted 1:1000 in either 5% nonfat milk in TTBS or 5% BSA in TTBS (for antibodies from Cell signaling). Membranes were washed three times with TTBS followed by incubation at room temperature for 1 h with secondary antibody (1:2000 dilution, anti-mouse/rabbit IgG coupled to alkaline phosphatase). Specific bands were detected by Thermo Scientific Pierce ECL

Western Blotting Substrate (Rockford, IL) and visualization was performed by exposure of the membranes to X-ray film. Densitometry was performed using ImageJ analysis software version 1.47v (NIH; *http://imagej.nih.gov/ij*). Samples were normalized to β-actin content and results are expressed as the means ± SD values of integrated optical density.

Measurement of cellular migration rate – On day 14 of ALI culture, well-differentiated HNEs were transferred to inverted microscope (Axio Observer, Carl Zeiss), equipped with a CCD camera (Axiocam 503, Zeiss) and an incubating chamber (Incustage, Live Cell Instrument), which maintained 37°C and 5% CO_2 level. Phase-contrast images of HNECs on apical plane were taken at 3-min intervals for 180 min. We calculated the two-dimensional instantaneous velocity field from the time-lapse images of migrating cells using open source software (PIVLab vs.1.41) written in MATLAB (Mathworks) (Thielicke and Stamhuis, 2014). Cross correlation matrix between each image was computed with discrete Fourier transform technique, where the size of interrogation window was set to 80 × 80 pixels for the first pass, 40 × 40 pixels for the second pass, and 20 × 20 pixels for the final pass with 50% overlap at each pass. From the acquired velocity map, distribution of migration speed was obtained with a binning window of 0.3 μm h^{-1}. Representative cell migration speed of each group was characterized by arithmetic mean of all vector magnitudes throughout the whole experiment.

Wound healing cell migration analysis – On day 14 of ALI culture, the HNEC layers were wounded with a sterile 200-μl pipet tip by one perpendicular linear scratch, creating a wound of $\sim$1 mm width across the diameter of the well. The wells were washed twice with PBS to remove detached cells or cell debris followed by incubation with the different stimuli. Images of the migrating cells were taken at 3-min interval for 18 h on the inverted microscope. We traced the position of migrating cell sheet boundary along x-axis at three different y positions. Instantaneous velocity of the leading front in x-axis,$v(t)$, was defined as $v(t) = \Delta t^{-1}(x_{t+\Delta t} - x_t)$, indicating change in position of the edge at time t (x_t) over the time interval Δt. To compare the initial behavior of cells after the scratch wound, velocity field of the leading front were acquired using PIVLab at different times (t = 15, 30, 60, and 120 min) after the scratch wound was inflicted. Interrogation window of 64 × 64 pixel with 50% overlap was used.

Quantification of cell shapes – Using Adobe Illustrator CS6, cell boundaries were manually traced over the fluorescently labeled actin images of HNECs acquired from confocal microscope. Cell shapes in xy plane were analyzed; cells without fully enclosed boundaries at the edge of images were neglected. We used a custom MATLAB script to compute cell shape index of each cell from the drawings of cell boundaries. Cell shape index (p) was calculated as $p = P/\sqrt{A}$ as previously defined (Bi et al., 2015), where P is is cell perimeter and A is cell area. The median of this shape parameter was computed.

Immunofluorescence staining – For cytospin slide preparation, cells were separated into single cells by incubation in non-enzymatic cell dissociation solution. Cells were cytospun on to the slides (500 cells per slide, 800rpm for 3 min).

For immunofluorescence staining, cytospins were fixed in cold methanol-acetone solution for 5 min and epithelial sheets on filters transwell-clear culture insert were fixed in 4% paraformaldehyde solution for 10 min and permeabilized in 1% Triton X-100 for 5 min. Either cytospins or epithelial sheets were incubated with the appropriate antisera (diluted 1:200 in DakoCytomation antidody diluent, respectively) overnight at 4°C, and then incubated with either secondary anti-mouse Texas red-conjugated IgG or secondary anti-rabbit FITC-conjugated IgG (1:250) for 1 h, or with FITC-phalloidin for 20 min at room temperature. After extensive washing, coverslips were mounted with VECTASHIELD Mounting Medium (Vector Laboratories, Burlingame, CA, USA) and analyzed by confocal laser-scanning microscopy (LSM700, Carl Zeiss MicroImaging GmbH, Jena, Germany).

Lentiviral transduction of HNE cells – Lentiviral particles containing the MISSION non-target *shRNA* control vector and *shRNA* vector targeting Furin (TRCN0000262167; NM_002569), PACE4

(TRCN0000075251; NM_002570), or β5 integrin (TRCN0000289121; NM_002213) were purchased from Sigma-Aldrich (St Louis, MO). Lentivirus transduction was performed in a 12 mm, 0.45 μm pore transwell-clear culture insert with 1×10^5 cells at a MOI of 5, following manufacturer's instructions (Sigma-Aldrich, St Louis, MO, USA).

Immunohistochemistry analysis – Formalin-fixed paraffin sections (4 μm) were de-waxed in xylene (Sigma Chemicals, St Louis, MO), rehydrated in successive ethanol baths, and subjected to antigen retrieval by microwave in 0.01 mol/L sodium citrate buffer (pH 6.0). Endogenous peroxidase activity was quenched with 3% methanolic hydrogen peroxide for 10 min at room temperature. Nonspecific binding was blocked by incubation with 10% normal serum from VECTASTAIN Elite ABC Kit (Vector Laboratories, Burlingame, CA) for 30 min at room temperature. Primary antibody (1:100 dilution) was applied at 4℃ for 24 h. Following washing in TBS, slides were incubated with horseradish peroxidase-conjugated species specific secondary antibody (1:5000 dilution, Vector Laboratories, Burlingame, CA) for 30 min at room temperature. Signal was amplified using the indirect immunoperoxidase technique using the DAKO Envision kit (Dako, Kingsgrove, Australia) Tissue sections were counterstained with Gill's hematoxylin (Sigma Chemicals, St Louis, MO), dehydrated, and mounted with DPX (ProSciTech, Thuringowa, Australia). Staining was visualized using an Olympus U-TV0.63XC microscope with the DP Controller software (Hamburg, Germany). The experiment was performed using four nasal mucosa specimens obtained from patients with allergic rhinitis.

Statistical analysis – Mean, median, and standard error values were calculated to assemble graphs using the Sigma Plot software version 10 (MMIV Systat Software, Inc., San Jose, CA) and the GraphPad Prism 3 for Windows (GraphPad software, La Jolla, CA, USA). Analysis of Variance and the unpaired student's t-test were used to analyze statistical significance between means. A probability less than 0.05 was considered significant.

Supplementary Figure Legends

Figure E1: IL-4 increases the expression levels of αv, β5, β6, and pFAK-Y925 regulated in the BC population. ***a***, Well-differentiate HNECs were treated with different IL-4 concentrations (0-20 ng/mL) to the basolateral compartment for 24 h. Cell lysates were immunoblotted with antibodies to αv, β5, β6, pFAK-Y925, and FAK. Beta-actin was used as a loading control. Note that β6 expression was significantly increased at IL-4 concentrations from 5 to 20 ng/mL, indicating that β6 expression is dependent on IL-4 dosage. ***b***, Well-differentiated HNECs were treated with or without IL-4 (5 ng/mL) and then used for cytospin preparations. Immunofluorescence double staining of cytospins was performed with control IgG (***upper panels***), anti-KRT5 and anti-αvβ5 (***middle panels***), and anti-KRT5 and anti-αvβ6 antibodies (***lower panels***). Note that αvβ5 and αvβ6 integrins were colocalizes with the basal cell marker KRT5 in IL-4-stimulated HNECs. Scale bar, 50 μm.

Figure E2: Periostin-αvβ5 integrin interactions are involved in IL-4-induced collective HNEC migration. ***a & b***, Well-differentiated HNECs were treated with either IgG control (10 μg/mL) or anti-periotin (10 μg/mL) in the presence or absence of IL-4 (5 ng/mL). The AP level of the HNEC layers was tracked by time-lapse video microscopy for 18 h at 3-min intervals. Images of moving HNECs were taken over the last 3-h period and calculated a displacement field per unit time using the PIV and determined the spatiotemporal velocity distribution within the HNEC layers. Mouse IgG was used as a control of anti-periostin. Heat map showing spatial distribution of velocity fields at a given instant (***left panels***) and quiver plots displaying speed and direction as arrows (***middle panels***). Scale bars, 50 μm (***a***). Confocal immunofluorescence of actin stained with phalloidin in HNECs treated with IL-4 for 24 h. Confocal x-y sections at the BL level of the HNEC layers were shown (***right panels***). Scale bars, 20 μm. Average HNEC migration speed. Values represent the mean ± SD, *** $P<0.0001$ by Student's t-test (***b***). All experiments were conducted on ALI cultures obtained from three different donors.

Figure E3: Anti-αvβ5 integrin induces anchorage loss-detachment cell death in IL-4-stimulated HNECs. Well-differentiated HNECs were treated with CMK, anti-αvβ5, or anti-αvβ6 in the presence or absence of IL-4 for 24 h and analysed by western blot using antibodies to caspase-3 and PARP. Beta-actin was used as a loading control. The data shown are representative of three independent experiments.

Figure E4: Integrins αvβ5 and αvβ6 in basal cells are required for IL-4-induced collective HNEC migration. ***a***, On day 2 of ALI, undifferentiated HNECs were treated with IgG control, CMK, anti-αvβ5, or anti-αvβ6, in the presence or absence IL-4, and tracked by time-lapse video microscopy for 18 h at 3-min intervals. Images of moving HNECs were taken over the last 3-h period and computed to measure the displacement field over time. Mouse IgG was used as a control of anti-αvβ5 and anti-αvβ6. Heat map showing spatial distribution of velocity fields at a given instant (***left panels***) and quiver plots displaying speed and direction as arrows (***right panels***). Scale bars, 50 μm. ***b***, Average HNEC migration speed. Values represent the mean ± SD, ** P<0.001 by Student's t-test. ***c***, Histogram of the velocity distribution for each group. Magnitude of the resulting velocity vectors was used to characterize velocity histogram of each group. The area of each histogram was normalized to the total number of velocity vectors in each group.

Supplementary Movie Legends

Movie E1
This movie shows wound closure monitored with time-lapse microscopy in control untreated HNECs. The length of the movie is 18 h - see Fig. 2 for full Legend.
Movie E2
This movie shows wound closure monitored with time-lapse microscopy in IL-4-stimulated HNECs. The length of the movie is 18 h - see Fig. 2 for full Legend.
Movie E3
This movie shows wound closure monitored with time-lapse microscopy in HNECs treated with IL-4 and CMK. The length of the movie is 18 h - see Fig. 2 for full Legend.
Movie E4
This movie shows collective cell migration monitored with time-lapse microscopy in control untreated HNECs. The length of the movie is 3 h - see Fig. 4 for full Legend.
Movie E5
This movie shows collective cell migration monitored with time-lapse microscopy in IL-4-stimulated HNECs. The length of the movie is 3 h - see Fig. 4 for full Legend.
Movie E6
This movie shows collective cell migration monitored with time-lapse microscopy in HNECs treated with CMK and IL-4. The length of the movie is 3 h - see Fig. 4 for full Legend.
Movie E7
This movie shows collective cell migration monitored with time-lapse microscopy in HNECs treated with anti-αvβ5 and IL-4. The length of the movie is 3 h - see Fig. 4 for full Legend.
Movie E8
This movie shows collective cell migration monitored with time-lapse microscopy in HNECs treated with anti-αvβ6 and IL-4. The length of the movie is 3 h - see Fig. 4 for full Legend.

References

Bi, D., Lopez, J. H., Schwarz, J. M., and Manning, M. L., 2015, A density-independent rigidity transition in biological tissues, *Nature Physics* **11**(12)**:**1074.

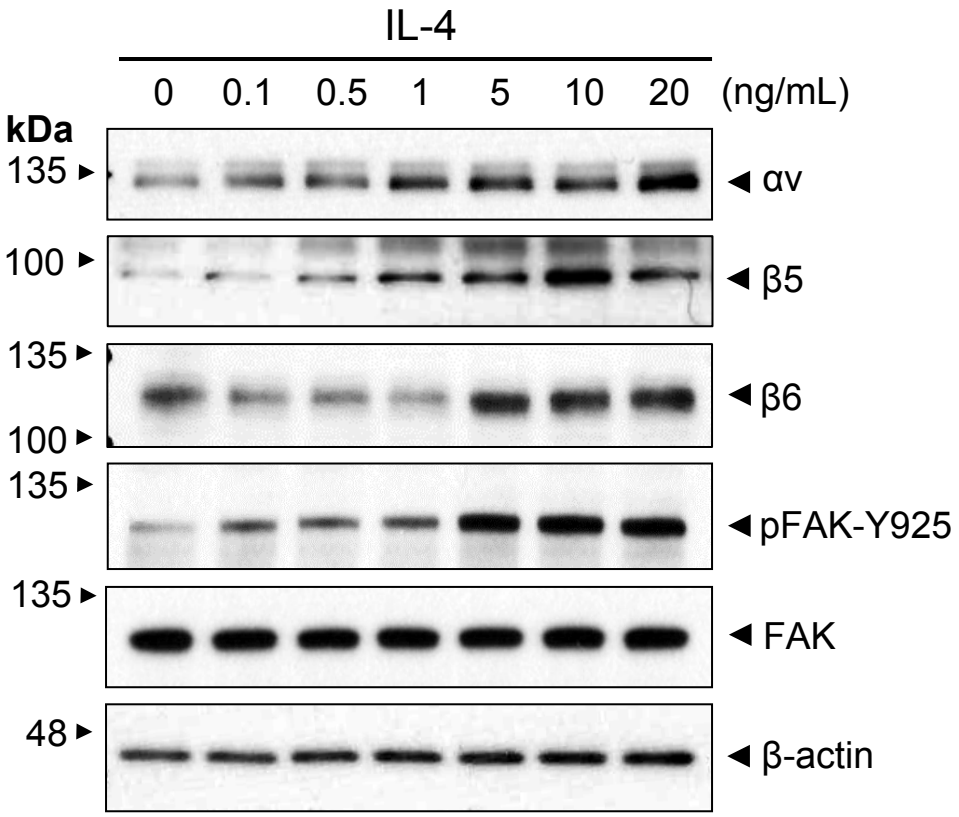
Thielicke, W and Stamhuis, E., 2014, PIVlab–towards user-friendly, affordable and accurate digital particle image velocimetry in MATLAB, Journal of Open Research Software, 2 (1): e30.

Yoon, J.-H., Kim, K.-S., Kim, H. U., Linton, J. A., and Lee, J.-G., 1999, Effects of TNF-a and IL-1 ß on Mucin, Lysozyme, IL-6 and IL-8 in passage-2 Normal Human Nasal Epithelial Cells, *Acta*

oto-laryngologica **119**(8)**:**905-910.

a

FIG. E1a
Lee et al



b

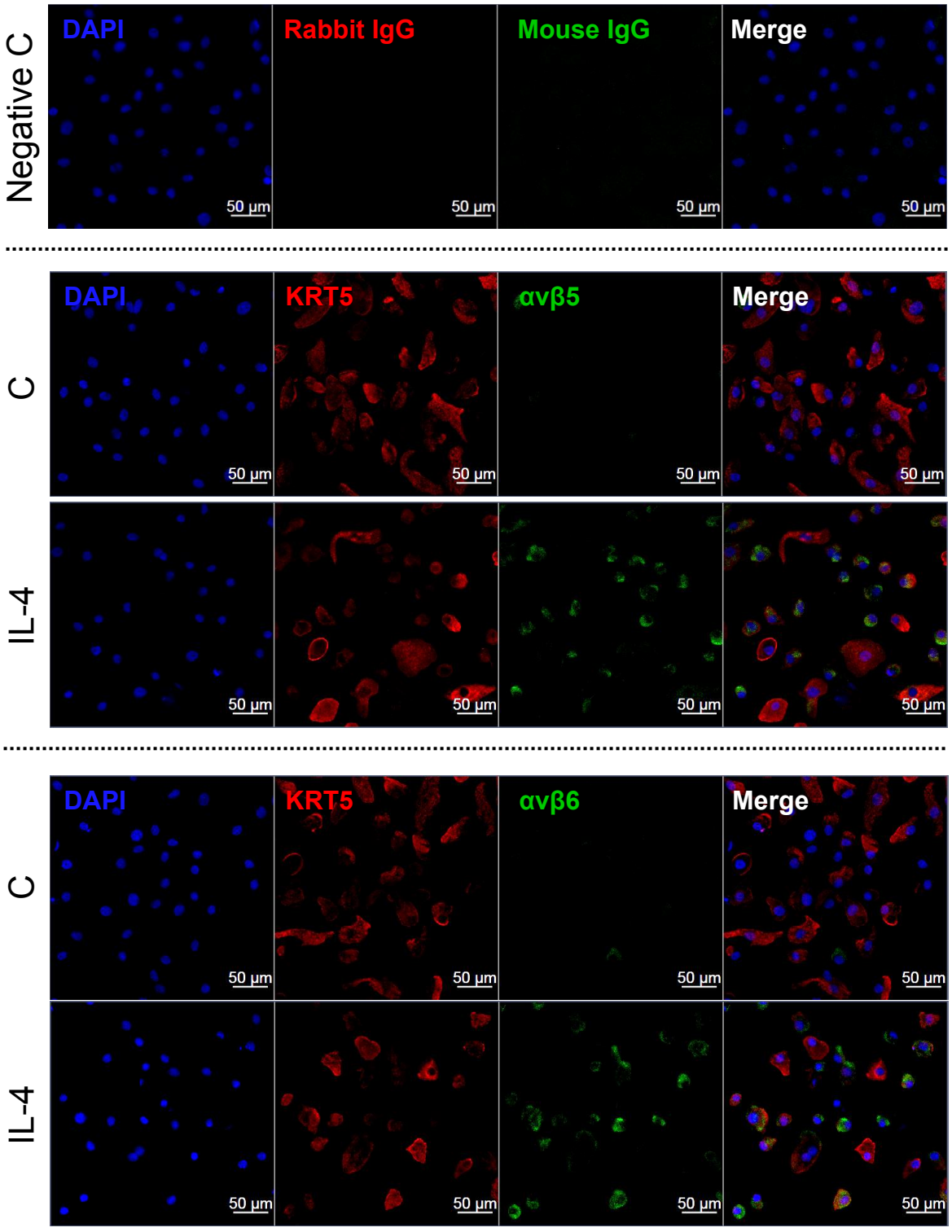

Negative C
DAPI
Rabbit IgG
Mouse IgG
Merge
C
DAPI
KRT5
αvβ5
Merge
IL-4
C
DAPI
KRT5
αvβ6
Merge
IL-4
50 μm

FIG. E2a
Lee et al

a

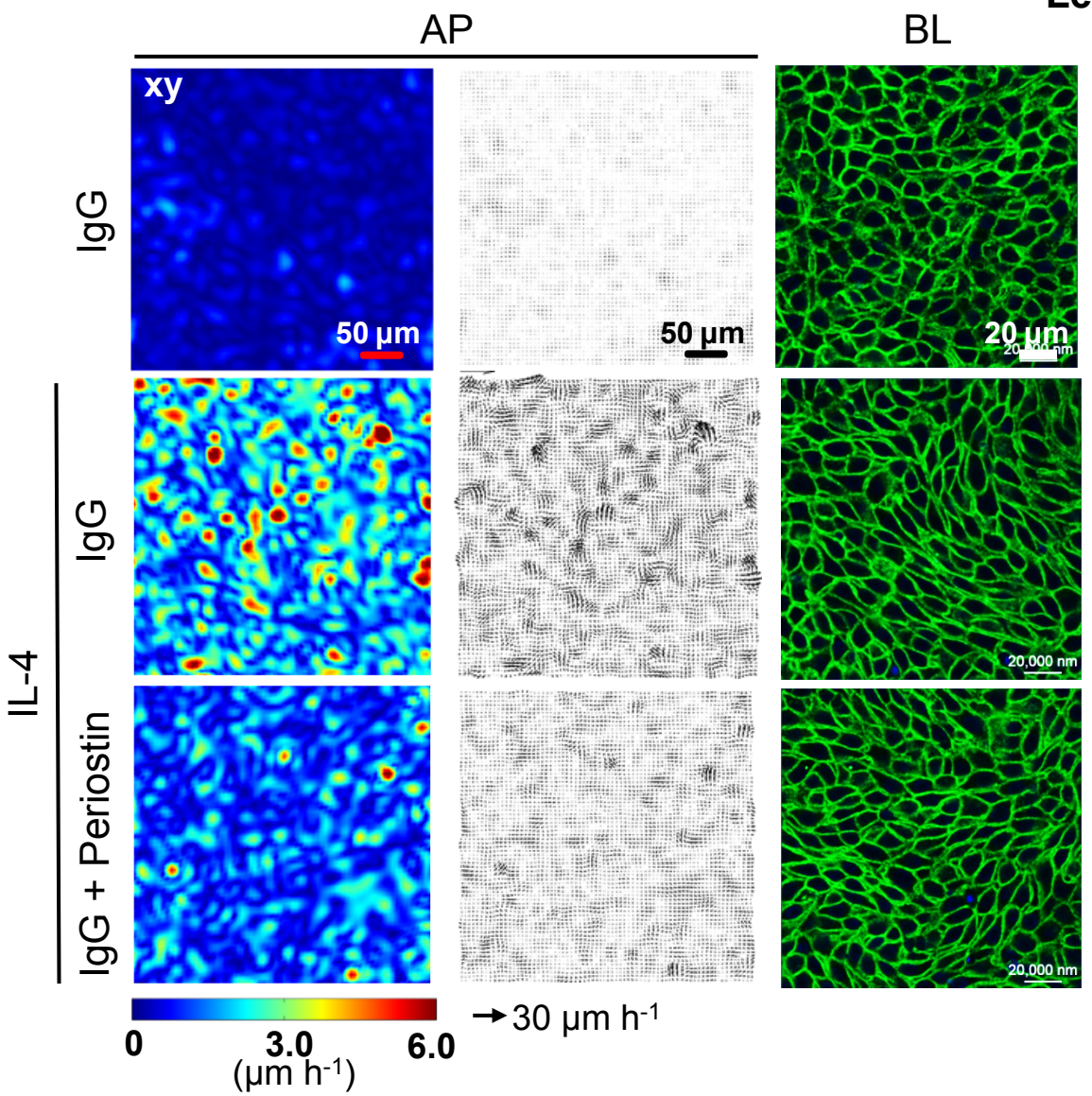


FIG. E2b
Lee et al

b

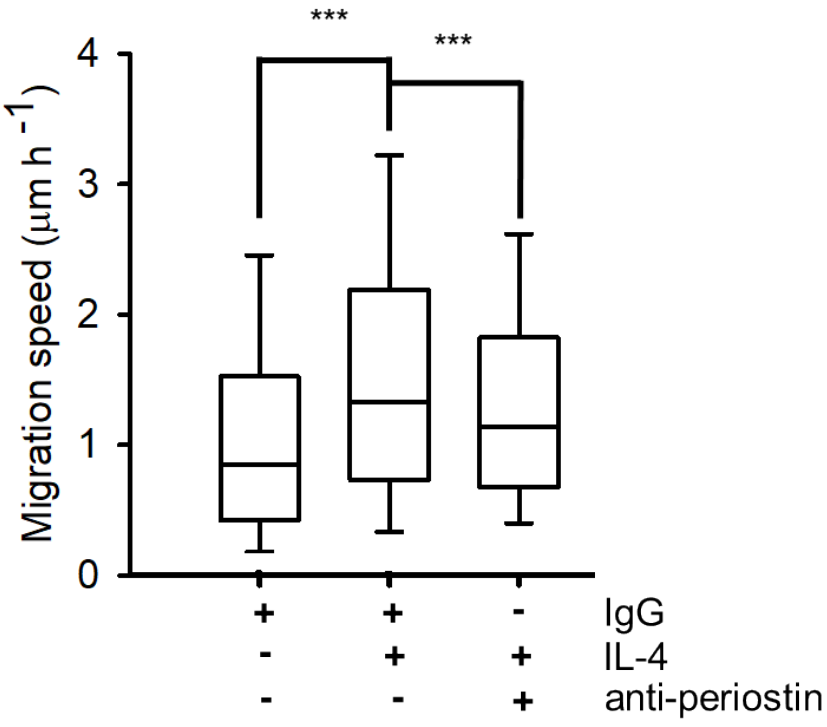
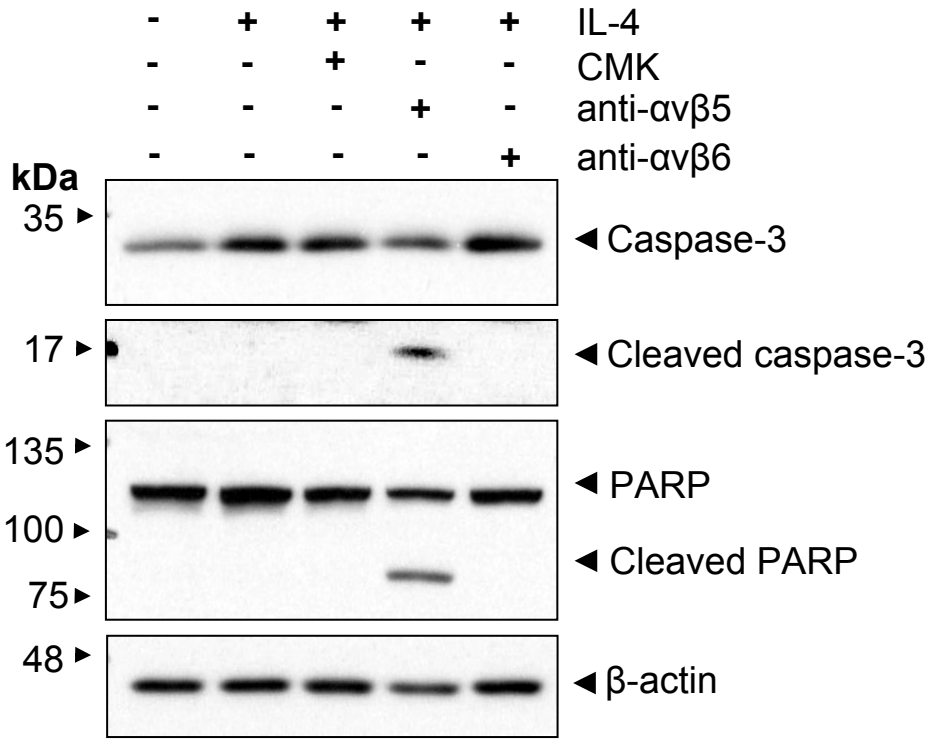


FIG. E3 Lee et al



a

FIG. E4a
Lee et al

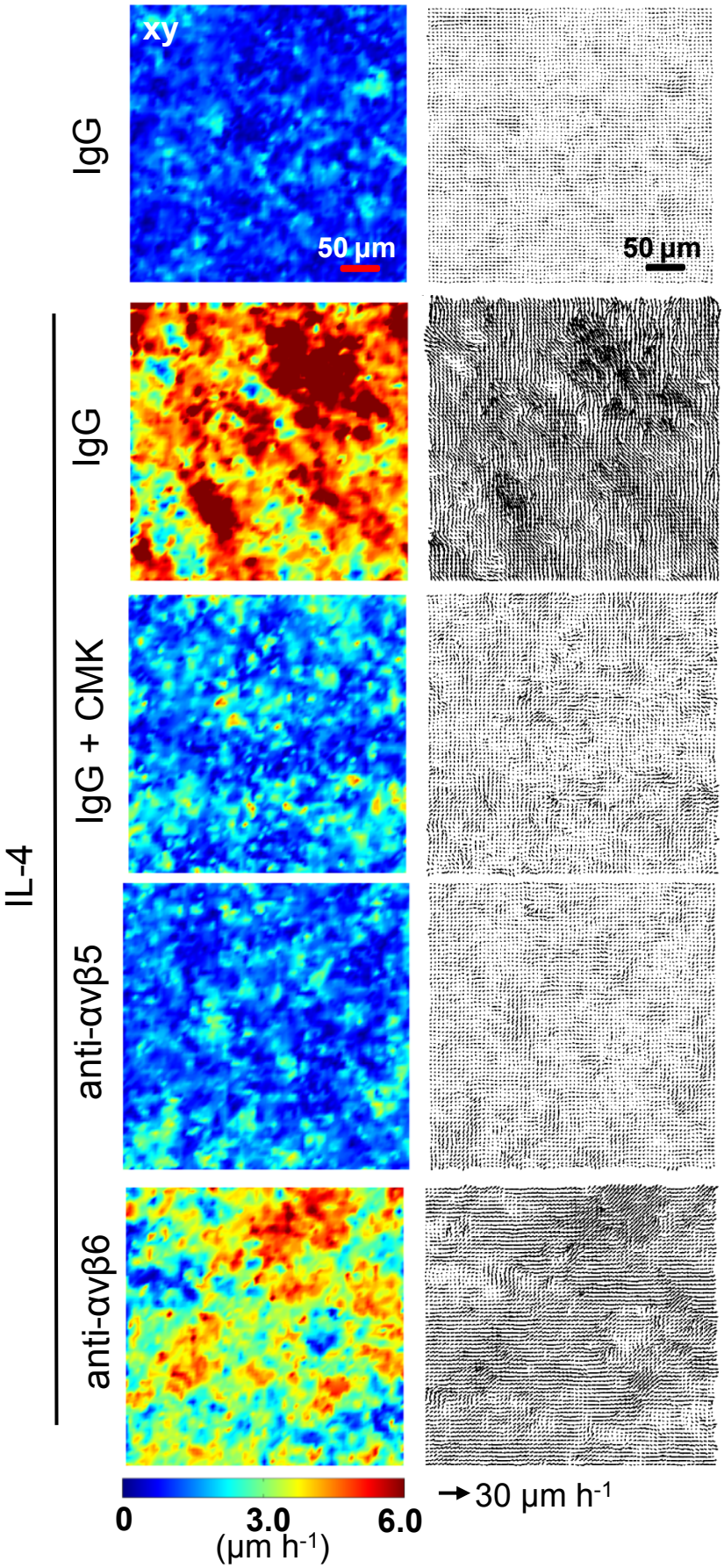
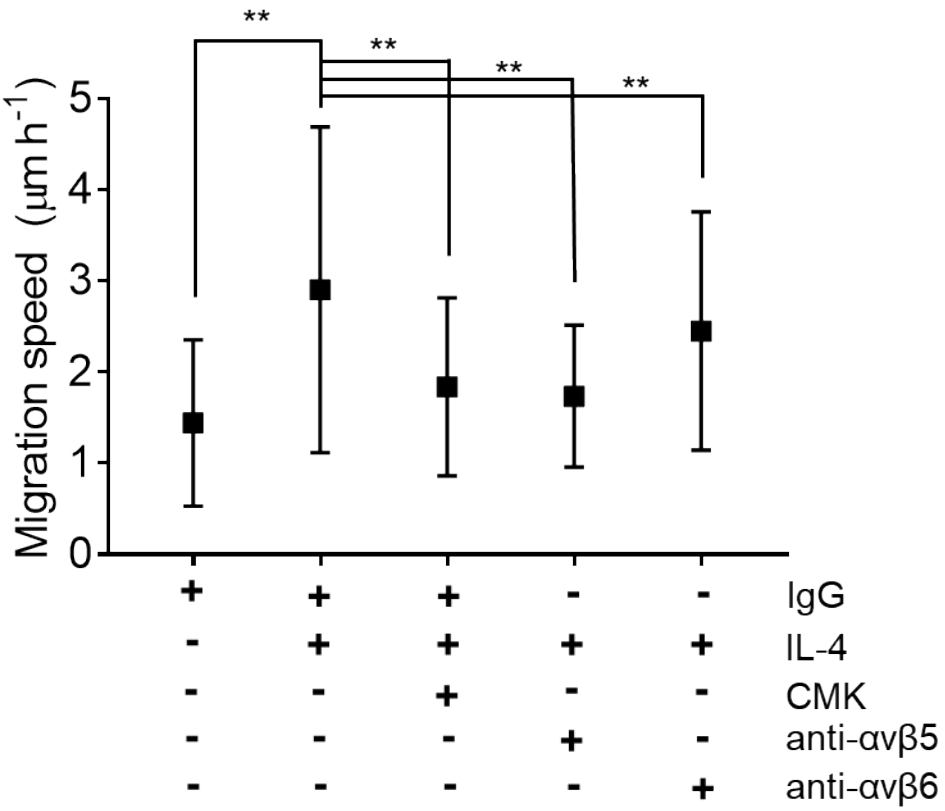


FIG. E4b&c
Lee et al

b



c

